

## **Supplementary Text: Details on S and Fe XANES analysis and data reduction**

**Article Title:** Variable oxidizing capacity of slab-derived fluids: insights from Fe and S speciation in glasses from the Troodos ophiolite

Saper, L.M., Brounce, M., Woelki, D., Cao, R., Bromiley, G.

### **Sulfur X-ray absorption near edge structure spectroscopy**

We determined  $S^{6+}/\Sigma S$  ratios of glass wafers by micro-x-ray absorption near-edge structure ( $\mu$ -XANES) spectroscopy at beamline 13-IDE, Advanced Photon Source, Argonne National Laboratory. Spectra were collected in fluorescence mode from 2447 eV to 2547 eV, with a dwell time of two seconds on each point, using a Si [111] monochromator and a beam with diameter of 15  $\mu\text{m}$ . Counts were recorded on a multi-element silicon drift detector x-ray spectrometer, equipped with two Si drift diode detectors. All analyses were done in a helium atmosphere to avoid interaction between the incident photon beam and atmosphere. Incident beam intensity was on the order of  $10^7$  photons per second per  $\mu\text{m}^2$ , reflecting a balance between the intensity required to produce interpretable S-XANES spectra from materials with low S-abundances (i.e., <3000 ppm) and the mounting evidence that very high photon density fluxes electronically damage Fe and S in silicate materials (e.g., Brounce et al. 2017; Cottrell et al. 2018; Lerner et al., 2021). Each analysis was performed using a stationary beam. S XANES spectra associated with each glass wafer are shown in the accompanying supplementary materials.

Spectral merging, background subtraction, and normalization was done using the X-ray absorption spectroscopy data software package ATHENA (Ravel and Newville 2005), applied uniformly to all spectra so that the region from 2447-2462 eV varies around a value of 0 and the region from 2485-2457 varies about a value of 1. These normalized spectra were then subject to a spectral fitting routine using the Fityk package to assess the suitability of a variety of approaches for reducing normalized S-XANES spectra to  $S^{6+}/\Sigma S$  ratios. Each normalized spectra was fit between 2462-2487 eV with four gaussian curves – one for the background (peak center fixed at 2485 eV) and one each for sulfate (peak center fixed at 2481 eV), the broad sulfide feature (peak center fixed at 2477 eV), and the narrow sulfide feature (peak center fixed at 2470 eV). The integrated  $S^{6+}/\Sigma S$  ratios reported in Supplementary Table 1 were calculated using the

area under the curves in three different ways. First, they were calculated assuming that the intensity of absorption features for both  $S^{2-}$  and  $S^{6+}$  respond linearly to the concentrations of  $S^{2-}$  and  $S^{6+}$  dissolved in the unknown samples. In this approach, the area under the gaussian centered at 2481 eV ( $S^{6+}$ ) was divided by the sum of the areas under the gaussians centered at 2481 ( $S^{6+}$ ) and 2477 ( $S^{2-}$ ) eV. In the second approach,  $S^{6+}/\Sigma S$  ratios were calculated using coefficients for absorption of 4.446 for  $S^{6+}$  and 1.864 for  $S^{2-}$  (i.e., acknowledging that the intensity of various absorption features may not respond linearly to the concentrations of  $S^{2-}$  and  $S^{6+}$  dissolved in the sample; Nash et al. 2019). In this approach, the scaled area under the gaussian centered at 2481 eV ( $S^{6+}$ ) was divided by the sum of the areas under the gaussians centered at 2481 ( $S^{6+}$ ) and 2477 ( $S^{2-}$ ) eV. The third approach again assumes that the intensity of absorption features for both  $S^{2-}$  and  $S^{6+}$  respond linearly to the concentrations of  $S^{2-}$  and  $S^{6+}$  dissolved in the unknown samples, and reports  $S^{6+}/\Sigma S$  ratios as the area under the gaussian centered at 2481 eV ( $S^{6+}$ ) divided by the sum of the areas under the gaussians centered at 2481 ( $S^{6+}$ ), 2477 ( $S^{2-}$ ), and 2470 ( $S^{2-}$ ) eV (i.e., after Konecke et al. 2019).

### **Iron X-ray absorption near edge structure spectroscopy**

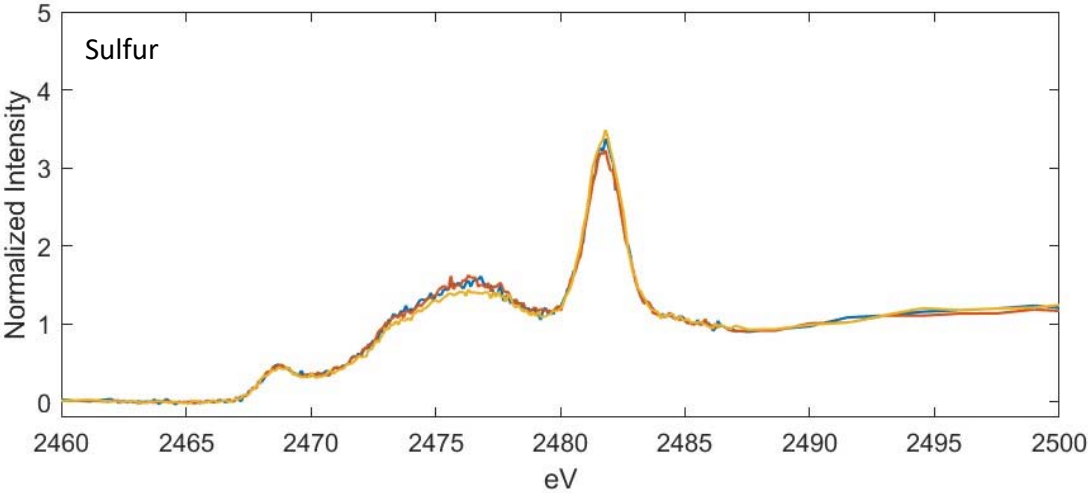
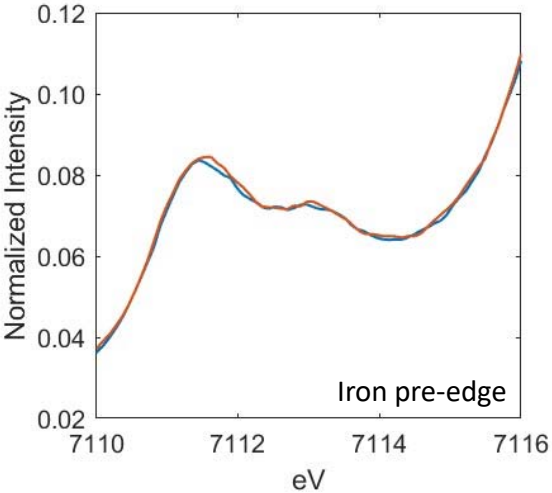
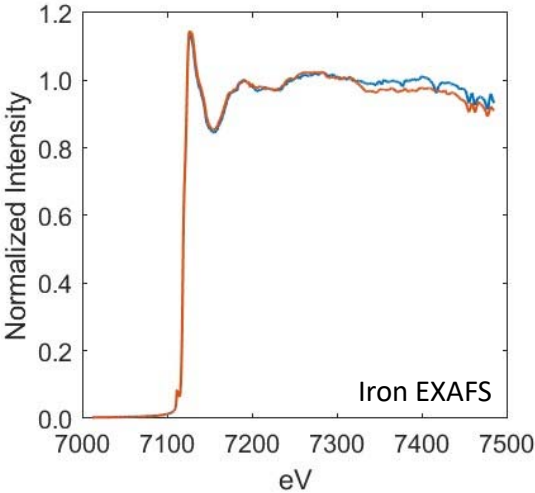
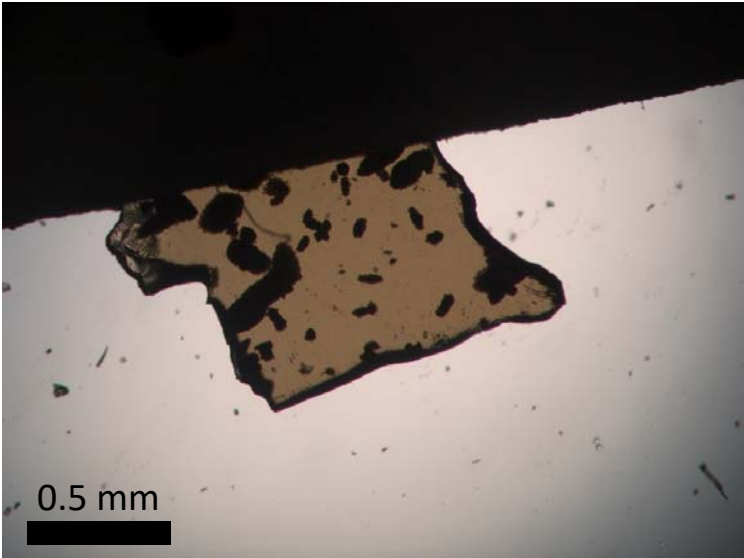
Measurements of the  $Fe^{3+}/\Sigma Fe$  ratios were made using Fe- $\mu$ -X-ray absorption near edge structure spectroscopy ( $\mu$ -XANES) at beamline 13-IDE at the Advanced Photon Source, Argonne National Laboratory following collection procedures described by Cottrell et al. (2018). Spectra were collected in fluorescence mode from 7012 eV to 7485 eV, with a dwell time of two seconds on each point, using a Si [111] monochromator and a beam with diameter of  $\sim 10 \mu m$ . Counts were recorded on a multi-element silicon drift detector x-ray spectrometer, equipped with two Si drift diode detectors. 100  $\mu m$  of aluminum foil was placed in the path of the incident photon beam in order to decrease the intensity of the incident photon beam to  $2 \times 10^9$  photons/second prior to interaction with the sample, which could lead to radiation-induced oxidation of Fe species dissolved in hydrous glass (e.g., Cottrell et al., 2018). During the analytical sessions, photo flux density at the sample surface was on the order of  $2 \times 10^7$  photons/second/ $\mu m^2$  or less. Fe XANES pre-edge and EXAFS spectra are shown for each glass wafer in the accompanying supplementary materials.

Spectra were normalized and fit according to methods described by Cottrell et al. (2009) and calibrated using standard glasses of Cottrell et al. (2009), with known  $Fe^{3+}/Fe^{2+}$  ratios

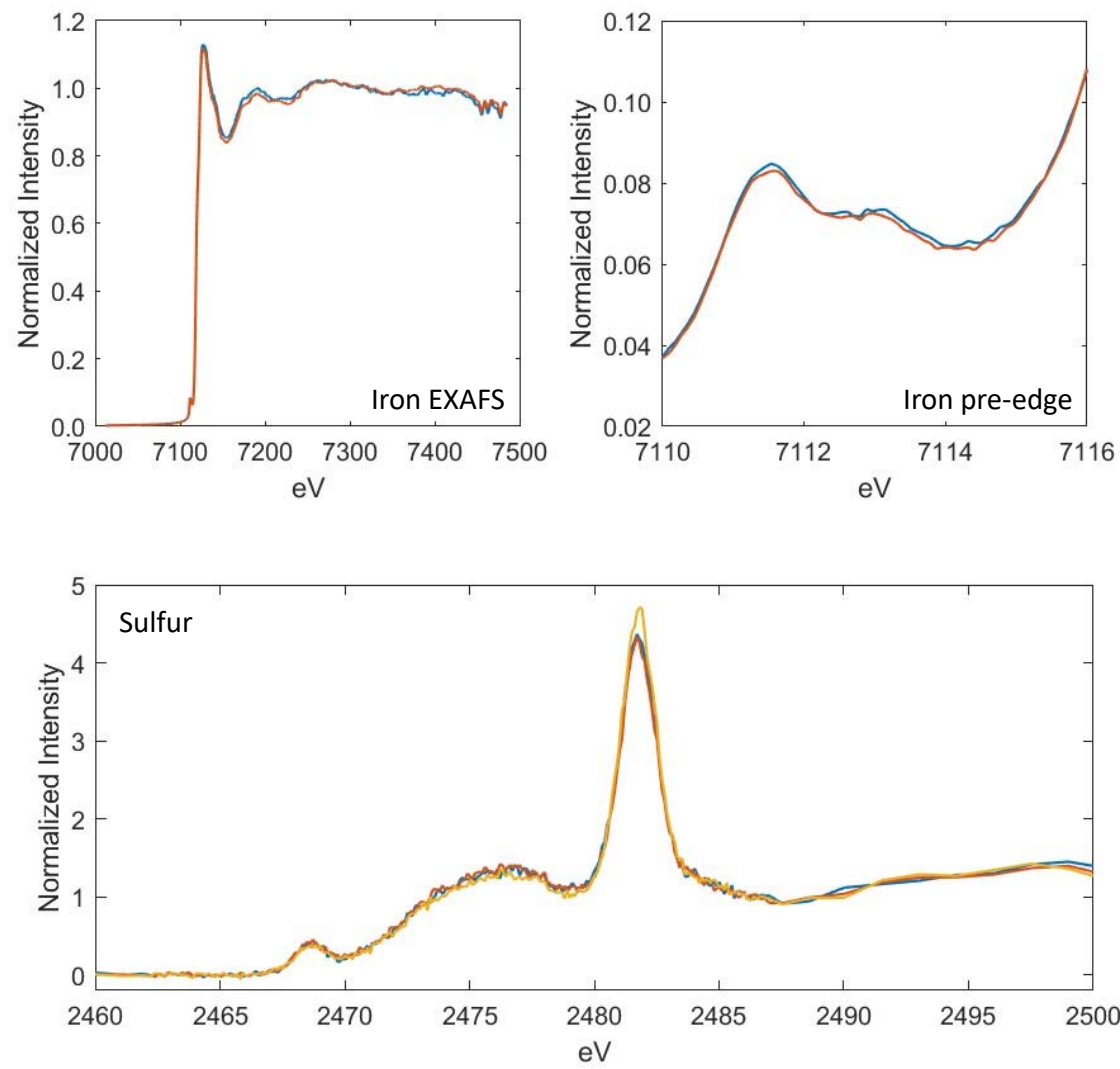
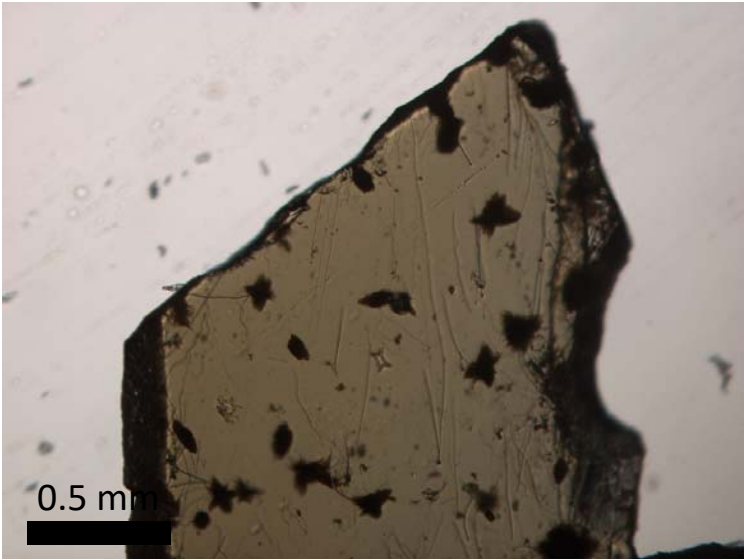
reported by Zhang et al. (2018a, 2018b). Edge-step normalization was applied uniformly to all spectra so that the region from 7012-7070 eV varies around a value of 0 and the region from 7200-7485 eV varies about a value of 1. The pre-edge regions of these normalized spectra were then subject to a spectral fitting routine using the Peak ANalysis (PAN) software package in an 8 eV window centered about the midpoint between the pre-edge peak that nominally appears at 7113 eV and the pre-edge peak that nominally appears at 7114.5 eV. These pre-edge regions were fit with a linear background and a DHO curve to flatten the pre-edge peaks. The pre-edge peaks were then fit with 2 gaussian features and the area weighted centroid position of these gaussian features was calculated for every standard and sample. The centroid position of repeated measurements of the standard LW-0 varied by +/- 0.02 eV across analytical sessions and all centroid positions were normalized to a corrected centroid position for LW-0 = 7112.30 eV. These corrected centroids were then used to calculate  $\text{Fe}^{3+}/\Sigma\text{Fe}$  ratios of samples according to the calibration of Zhang et al. (2018). We note that if we instead used the Mössbauer calibration of Berry et al. (2018) to reduce our Fe XANES data, our conclusions and interpretations remain unchanged.

**Optical images of each glass wafer and corresponding Fe and S XANES spectra are included in the following pages:**

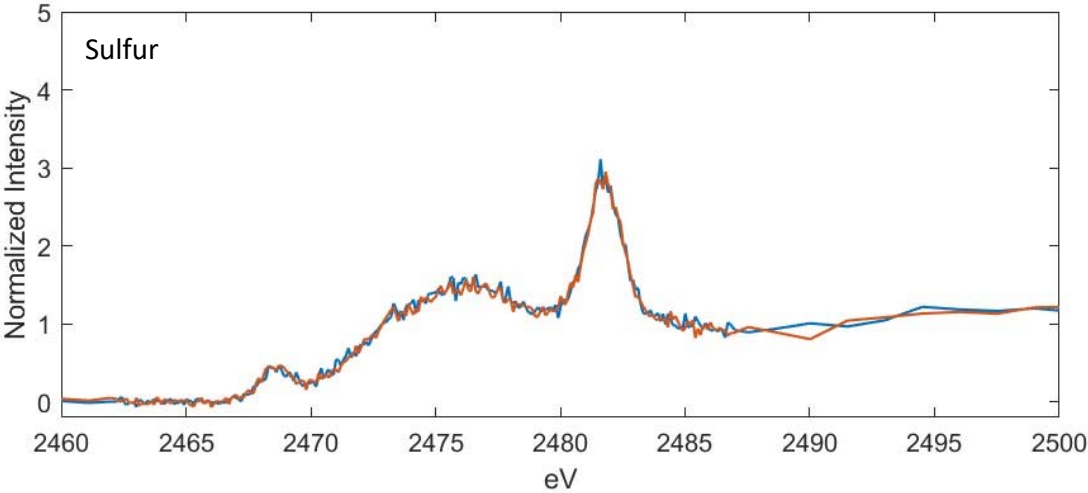
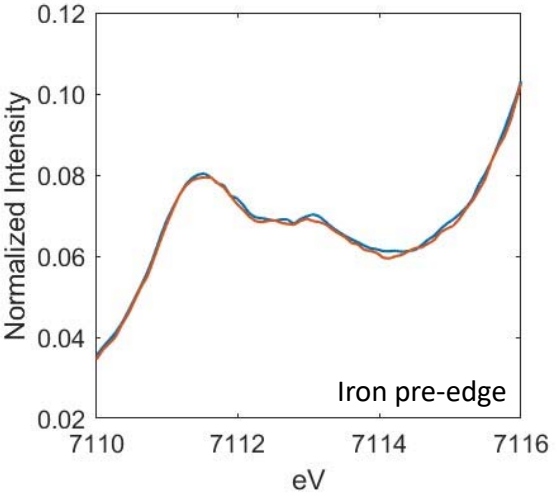
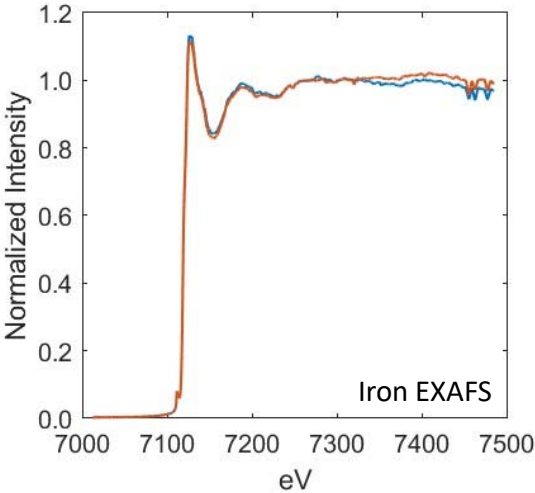
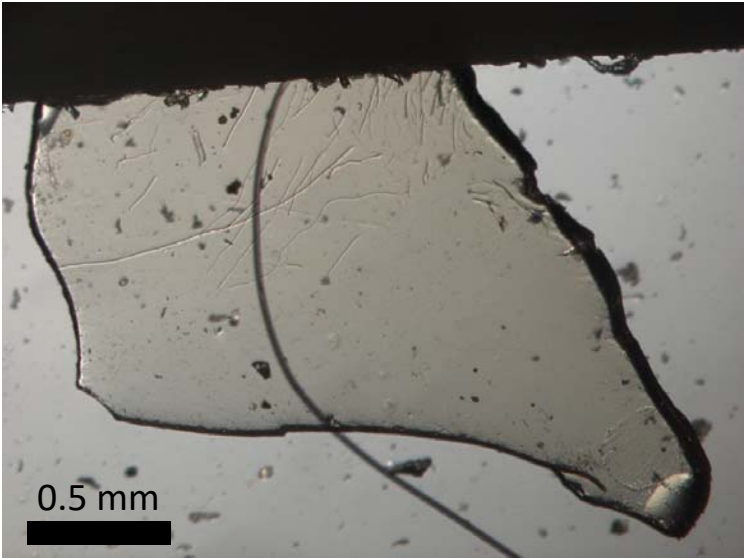
CY16-glass89



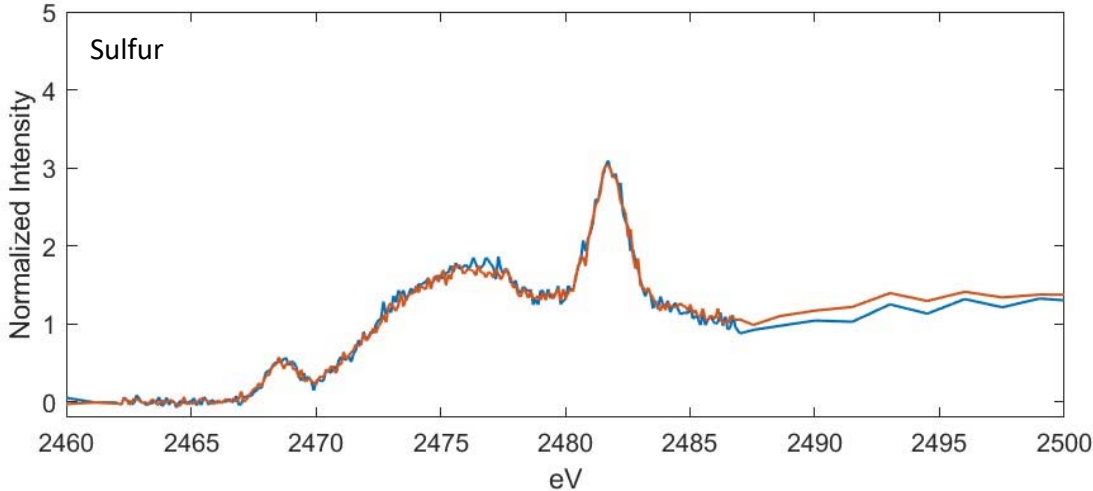
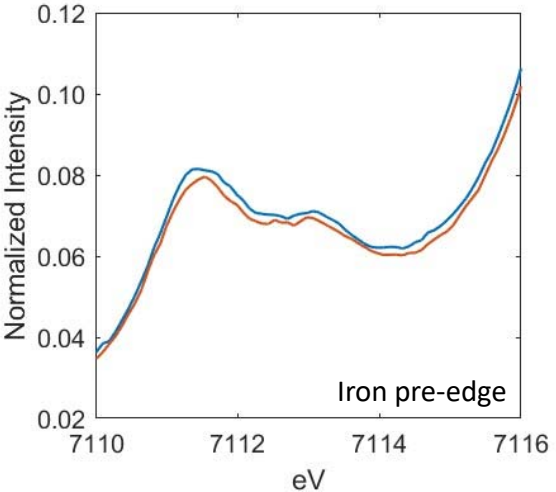
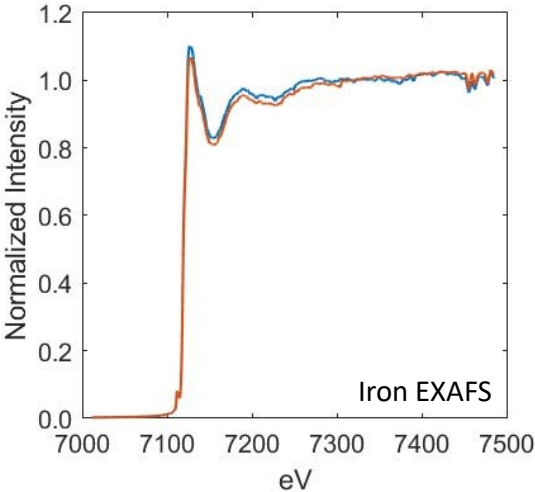
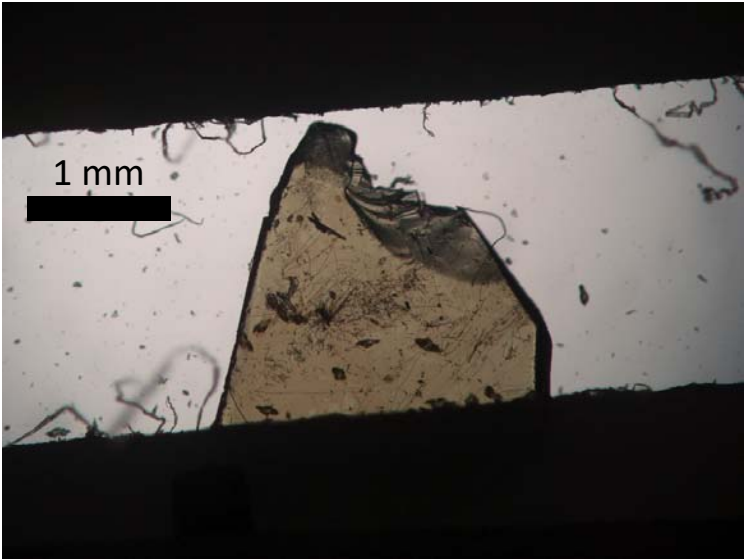
CY16-glass95



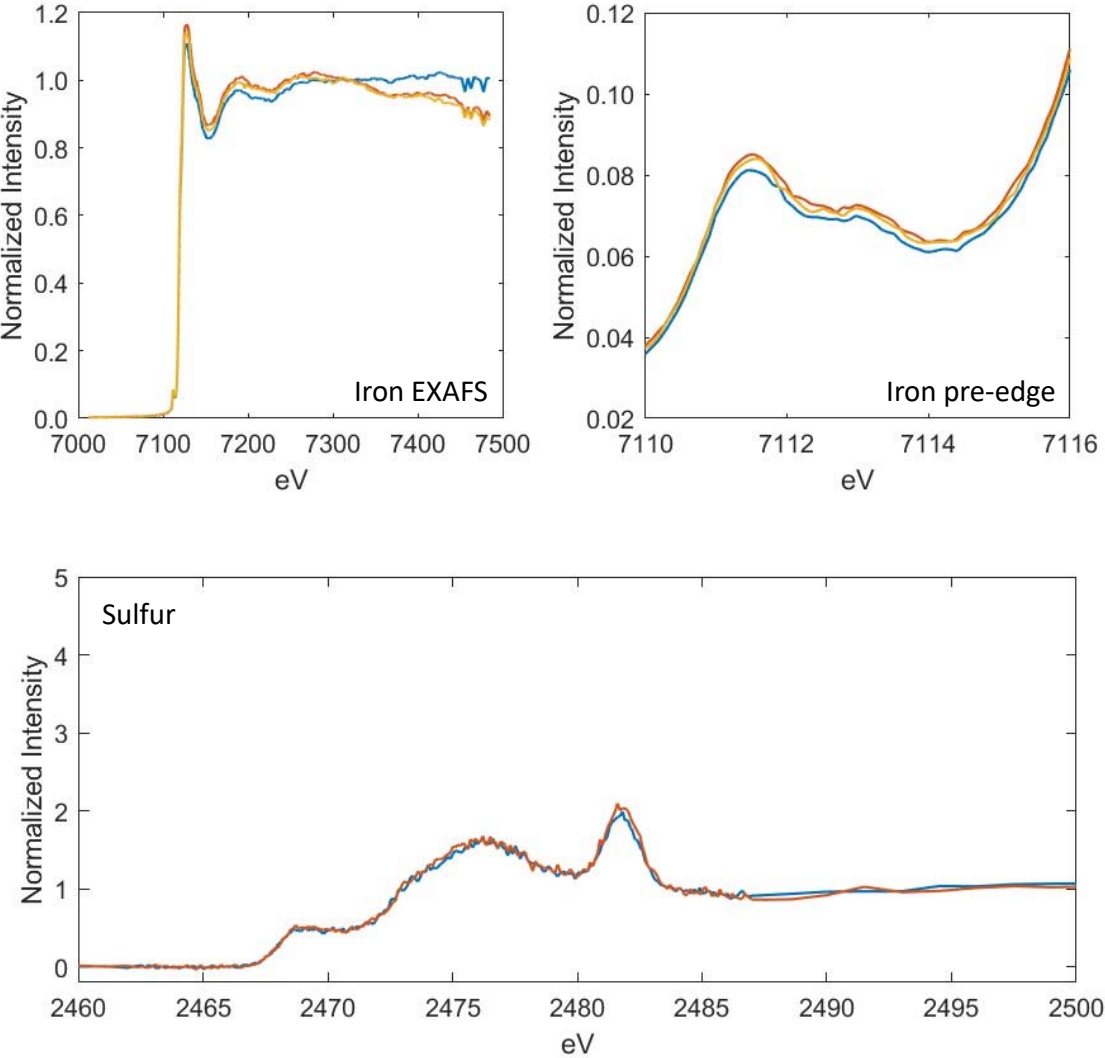
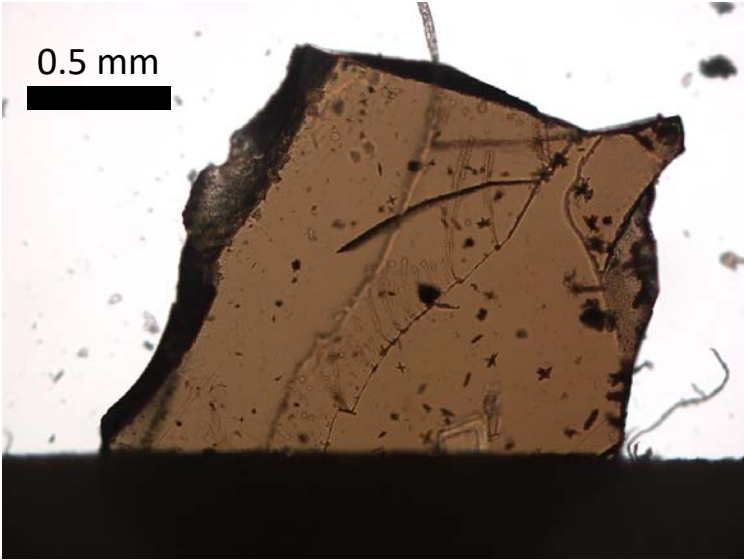
CY16-glass129



CY16-glass30

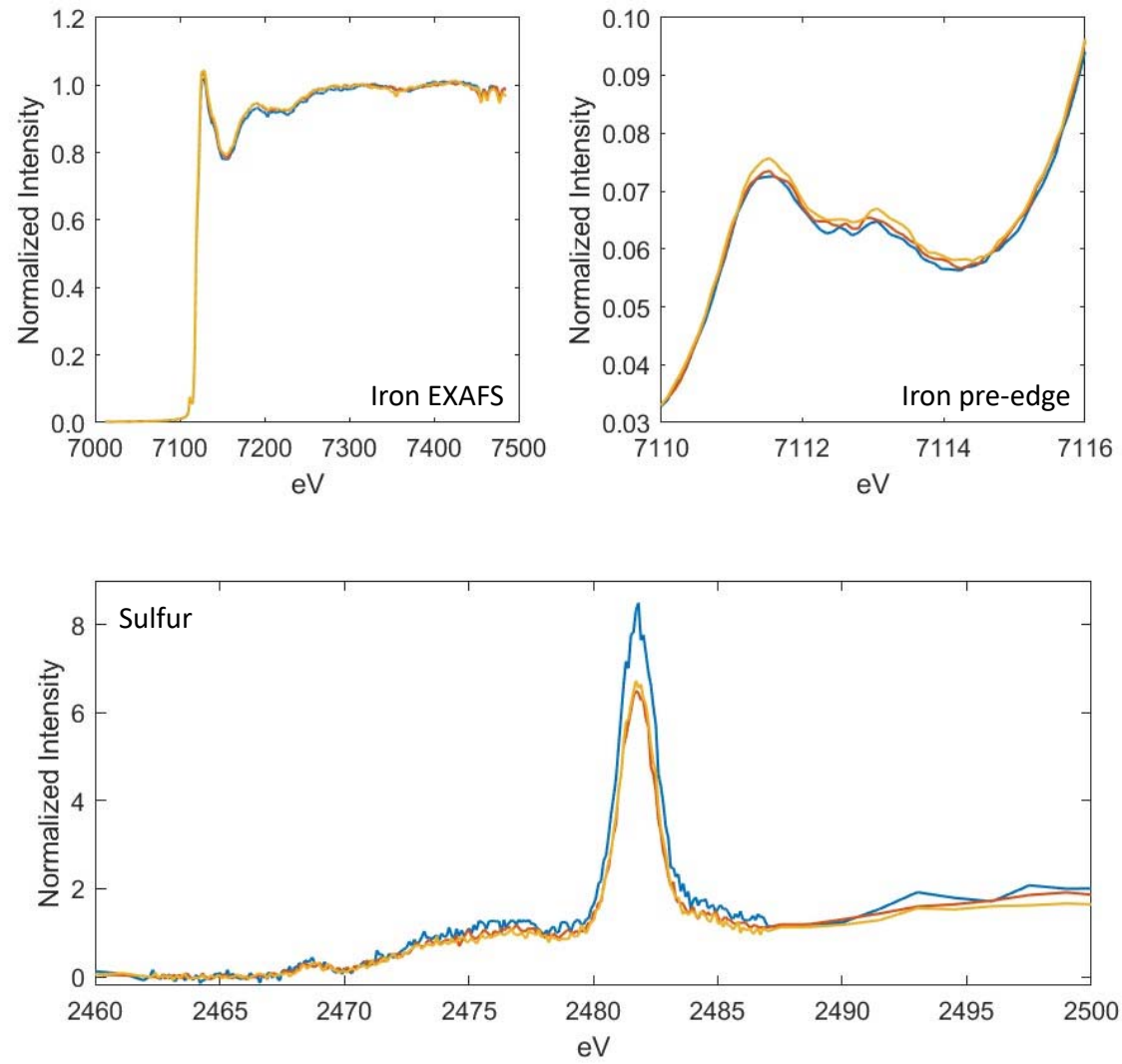
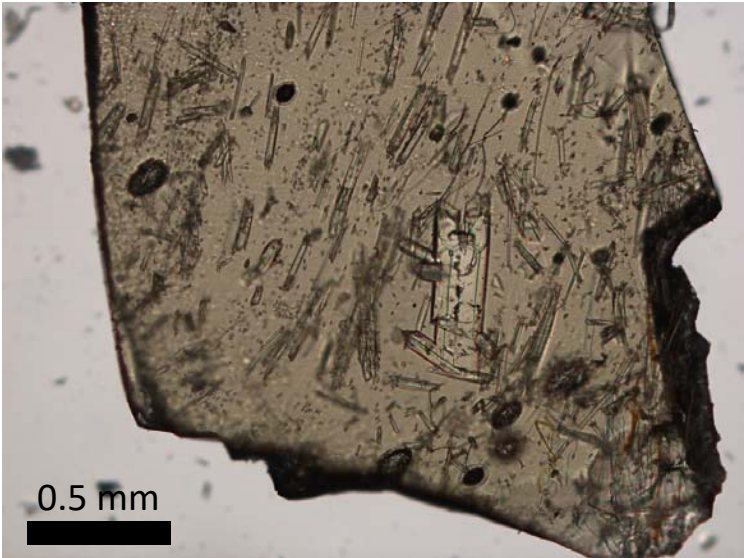


CY16-glass144

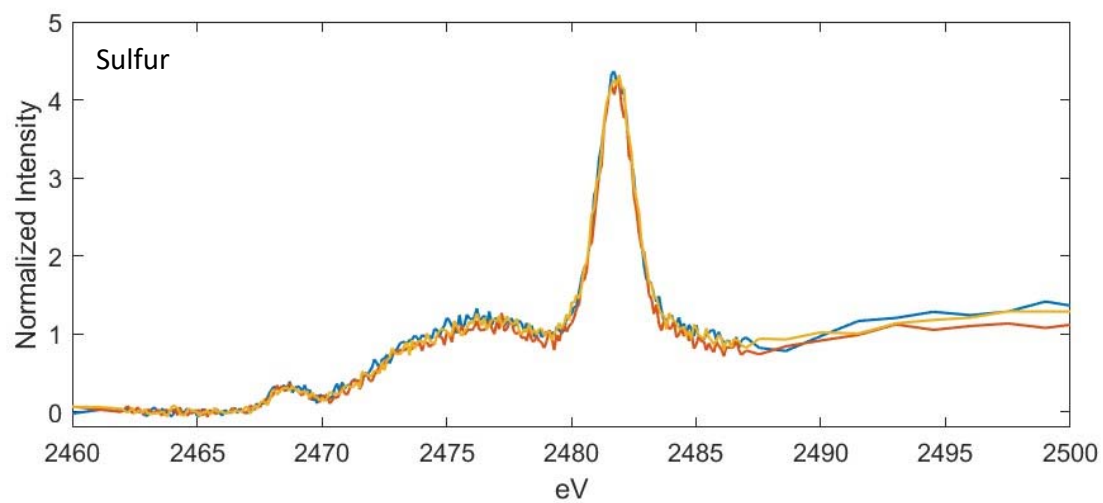
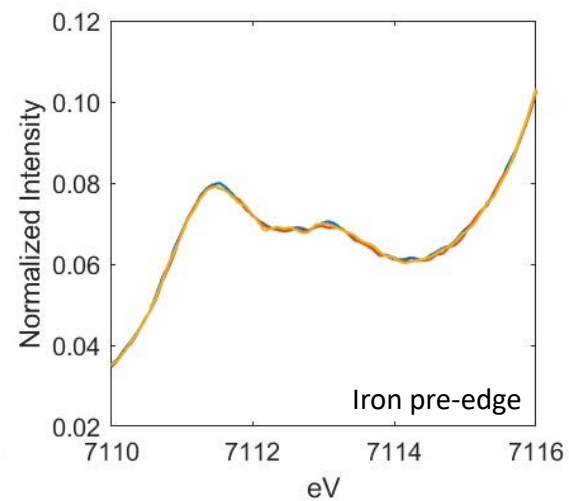
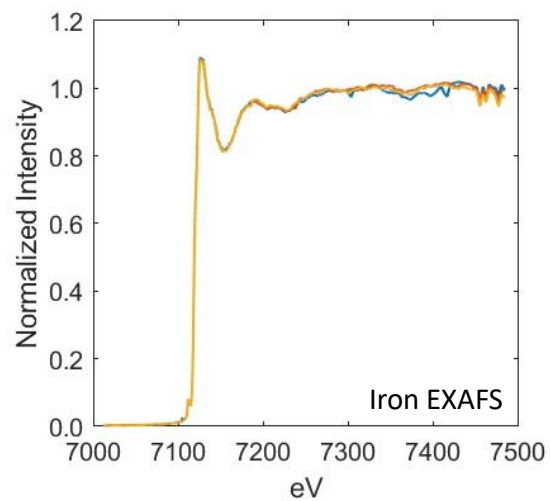
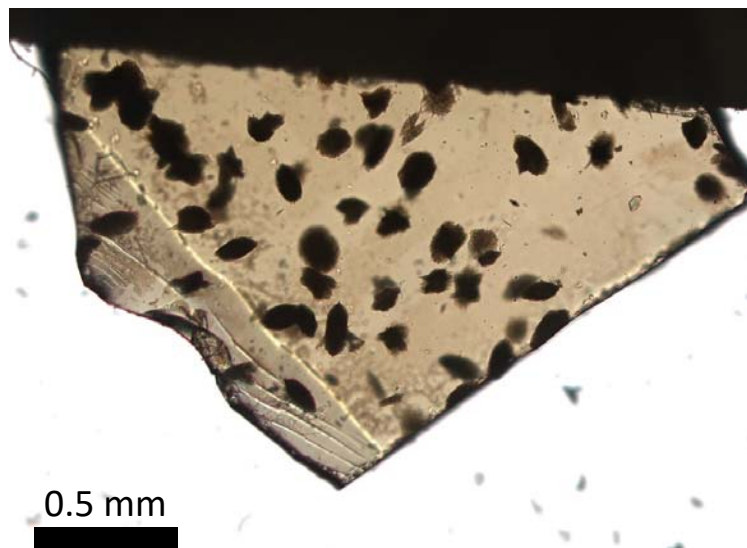




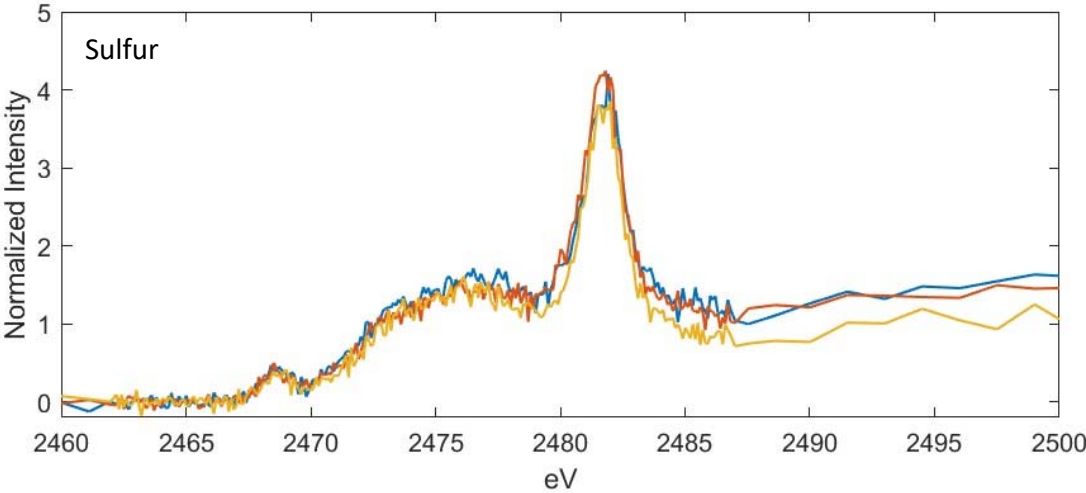
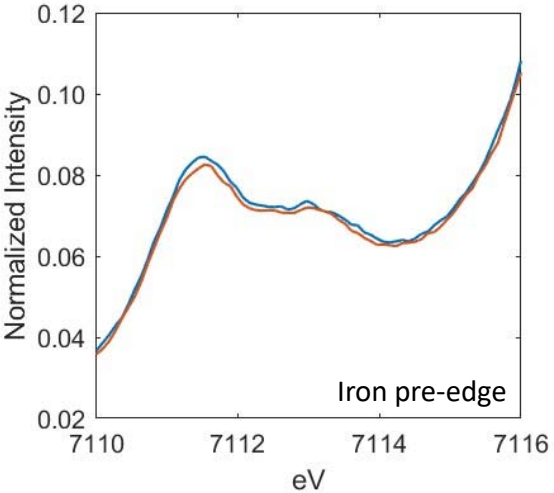
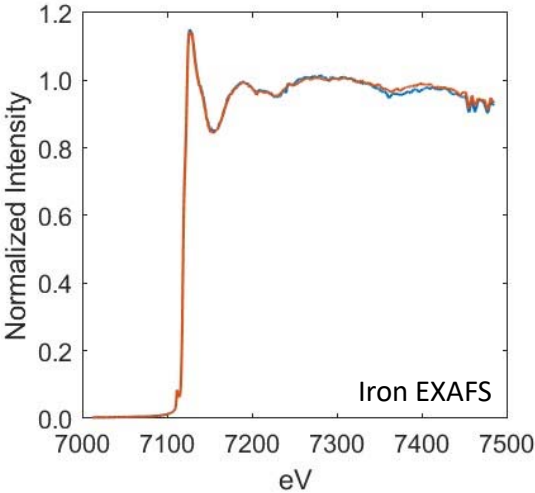
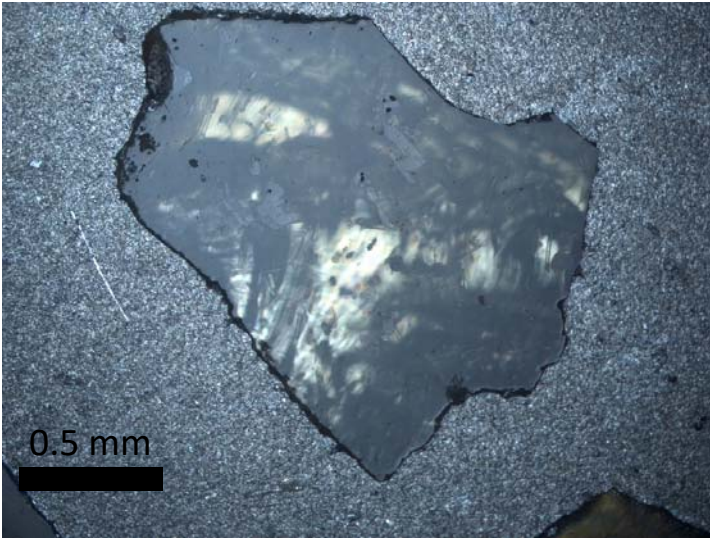
CY16-glass35



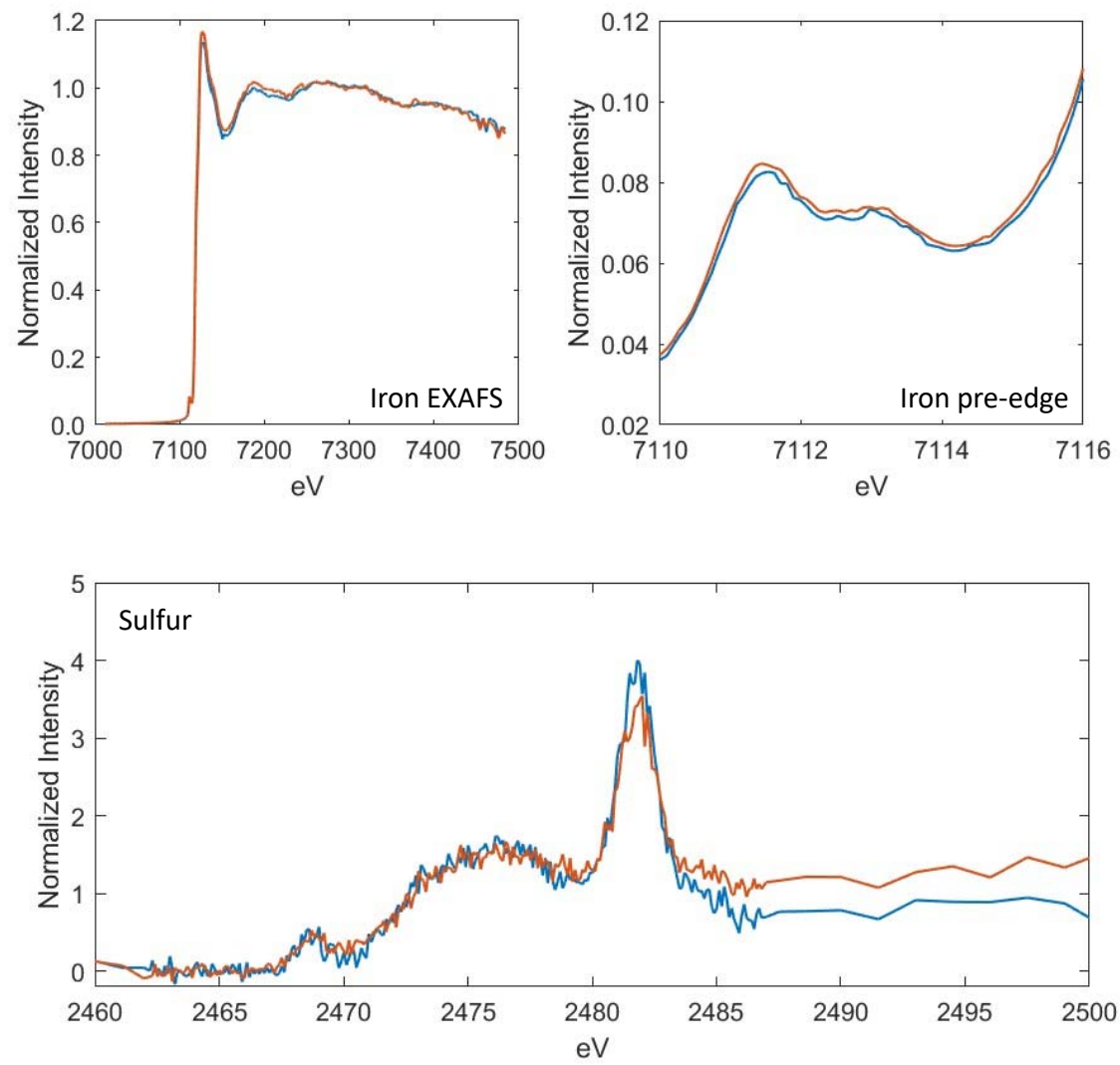
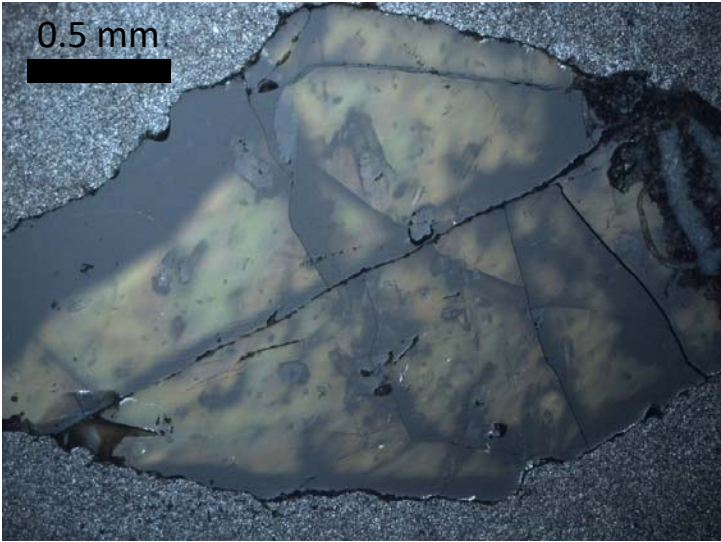
CY16-61



CY16-glass37

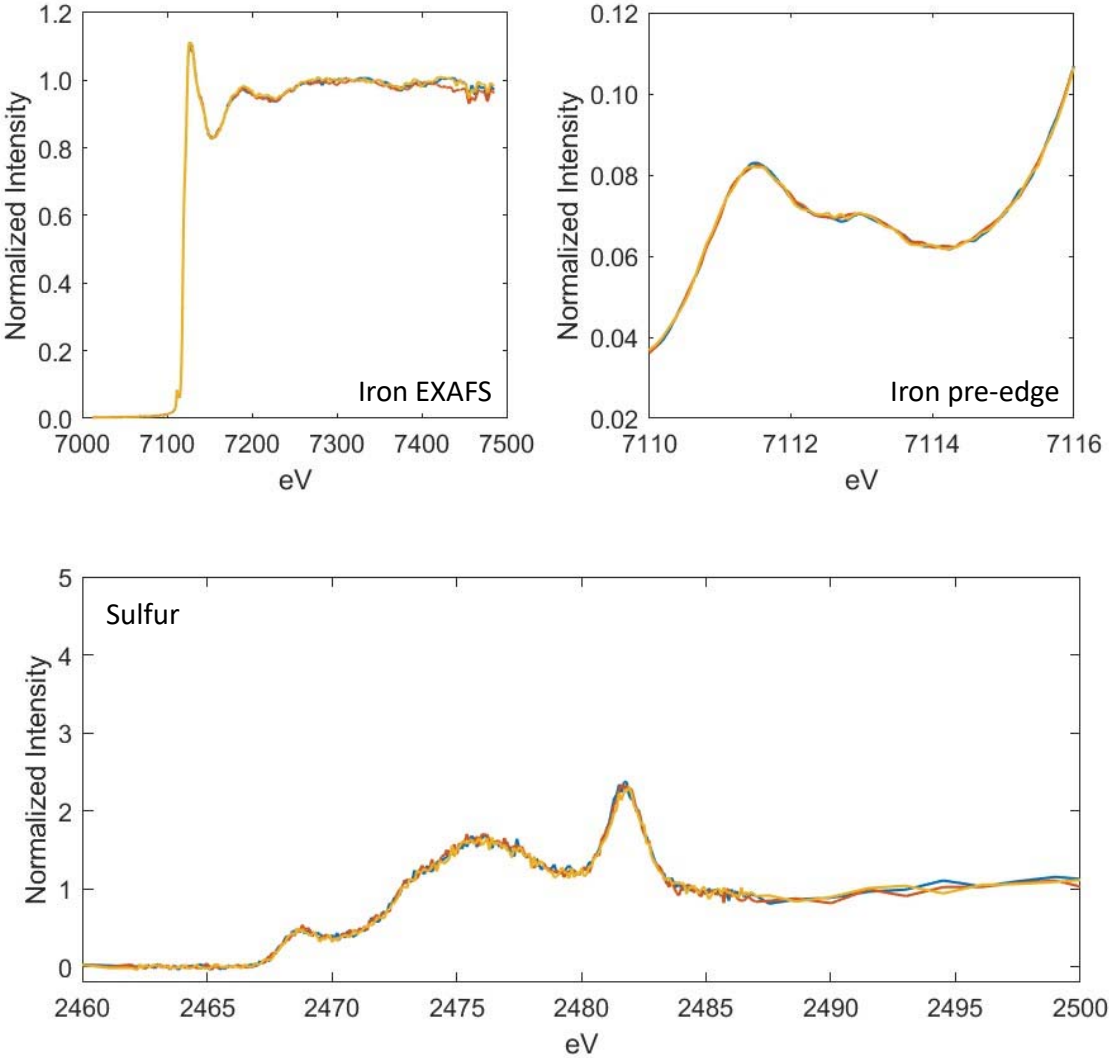
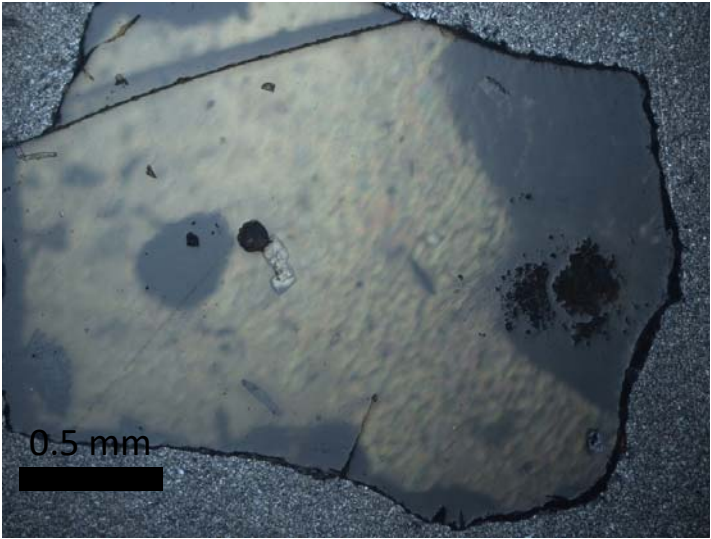


CY16-glass12

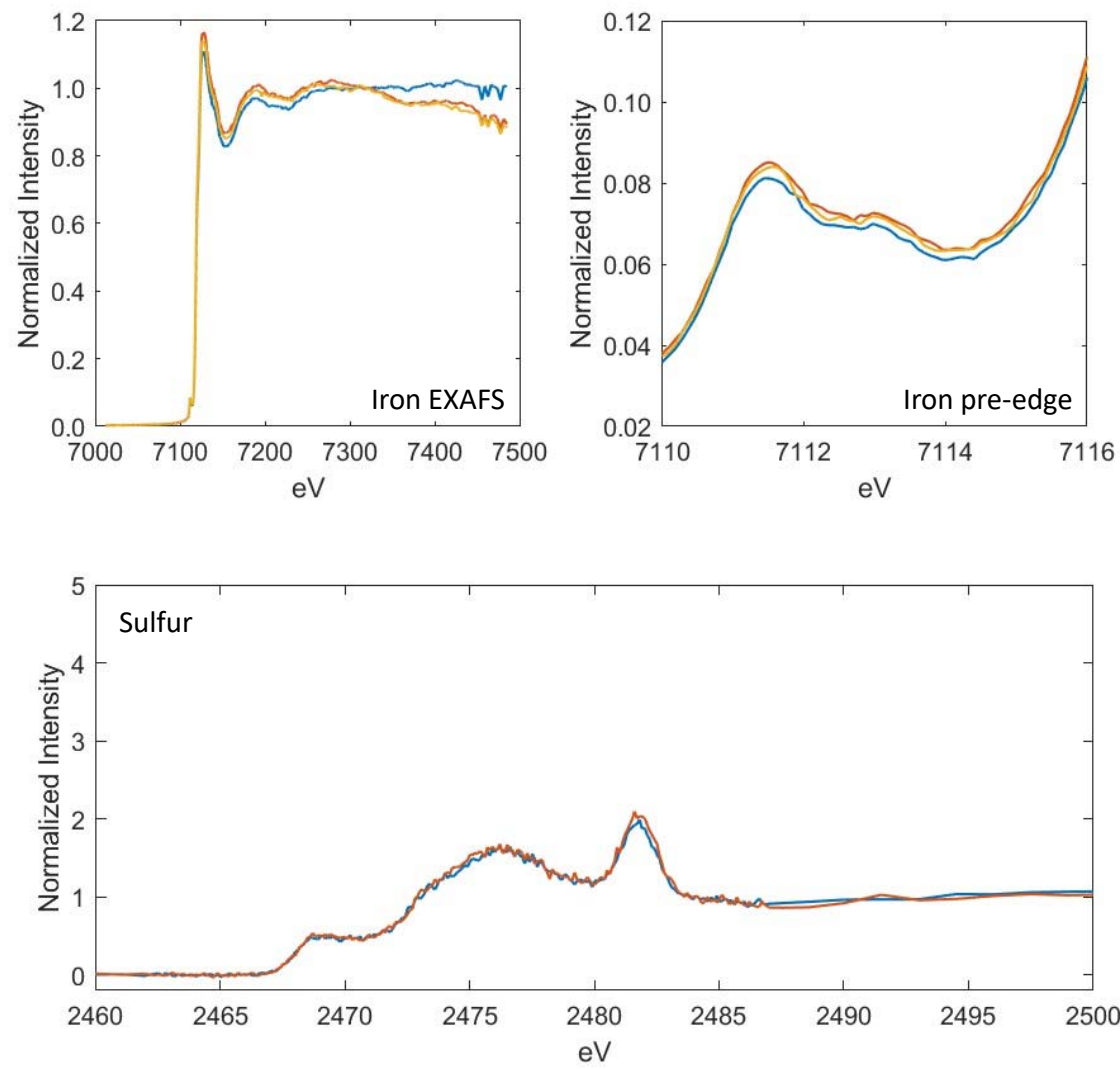
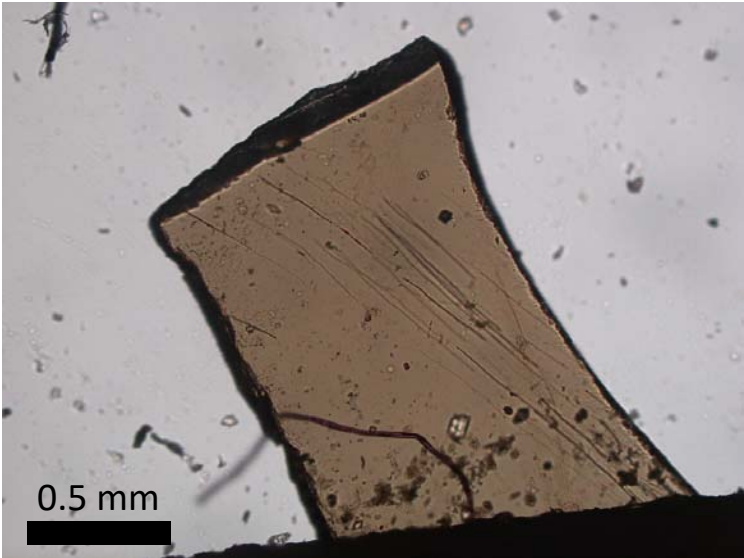




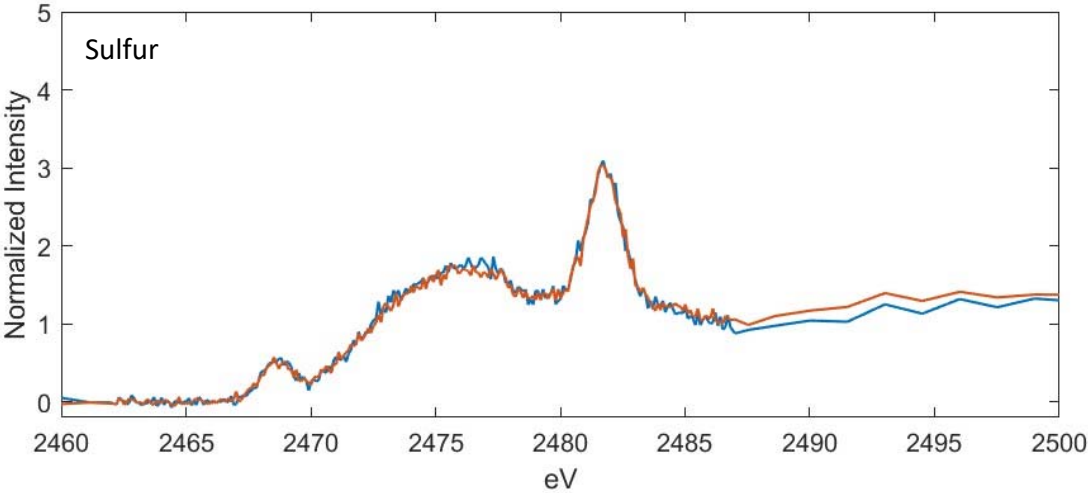
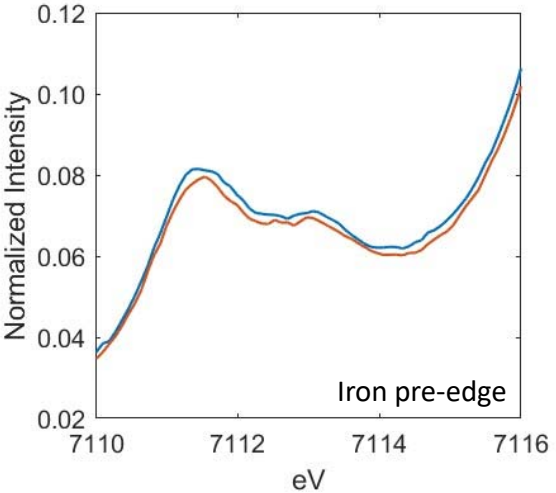
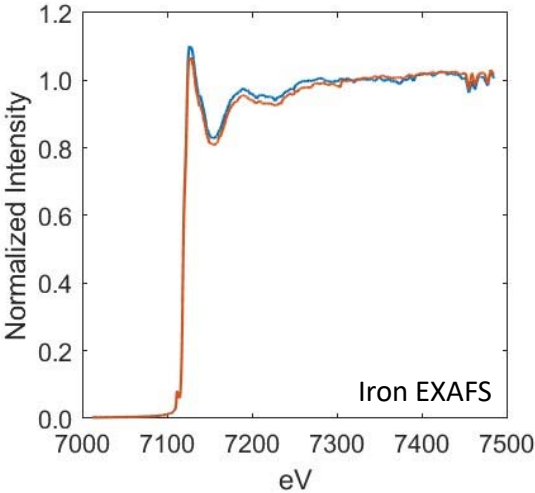
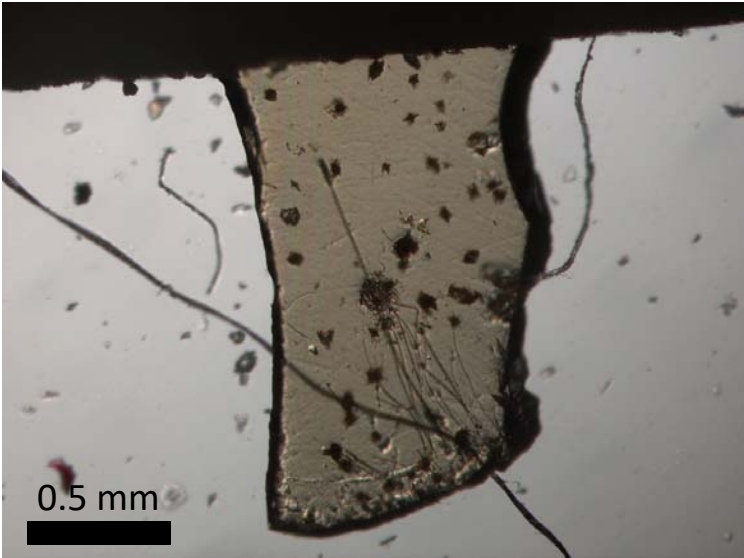
CY16-glass135



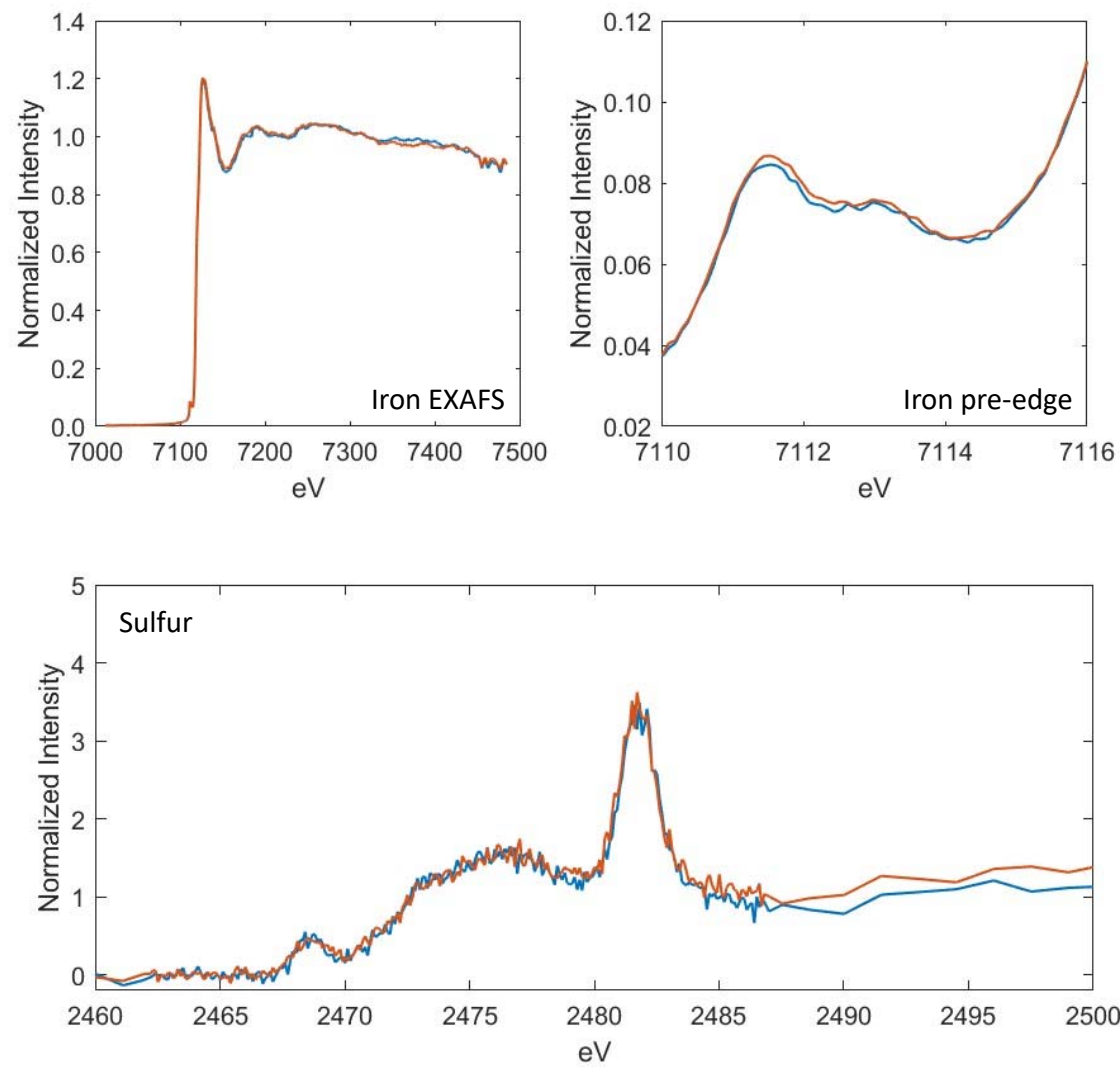
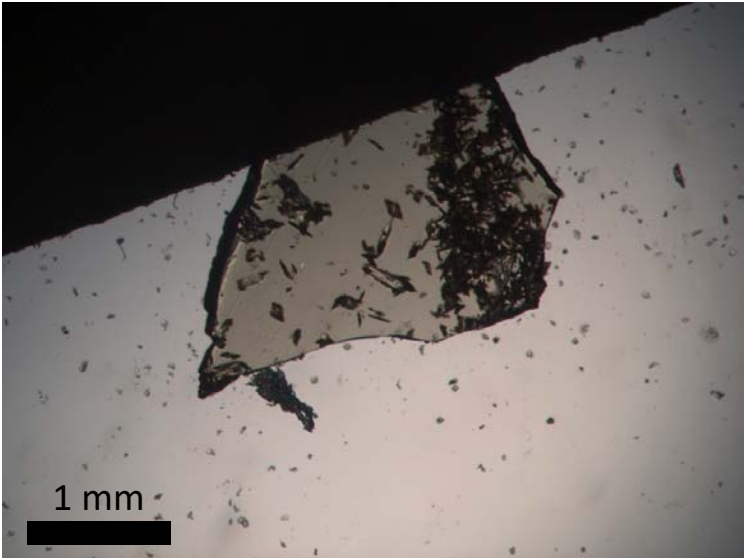
CY16-glass150



CY16-glass184

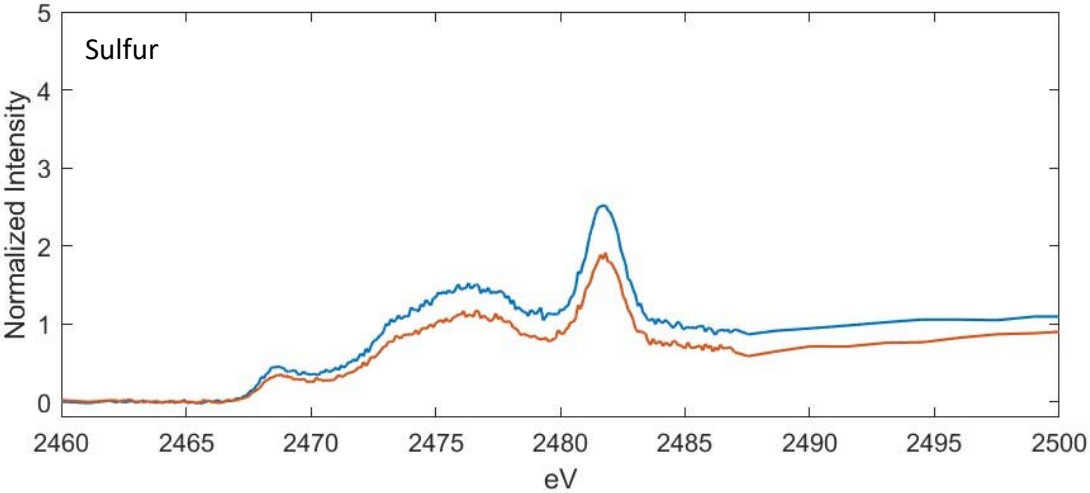
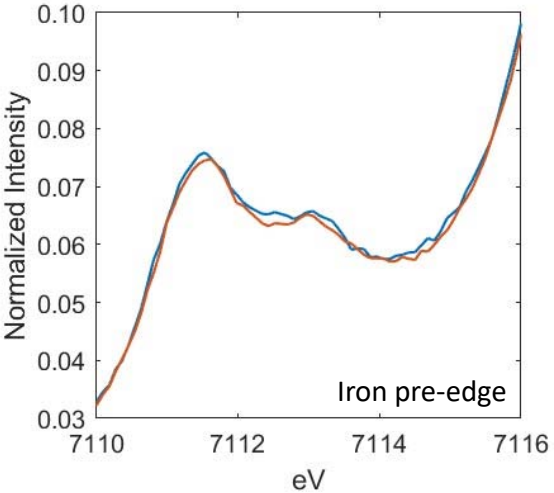
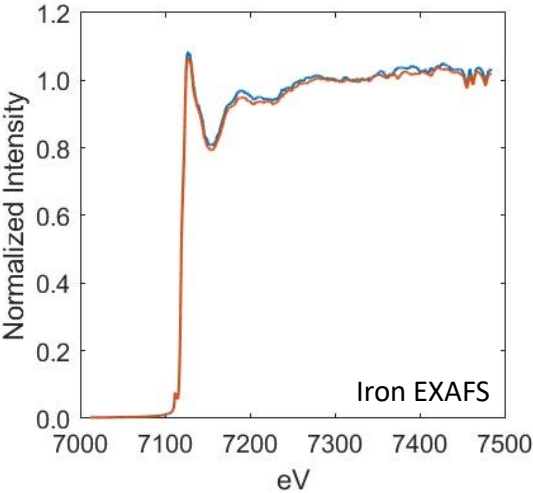
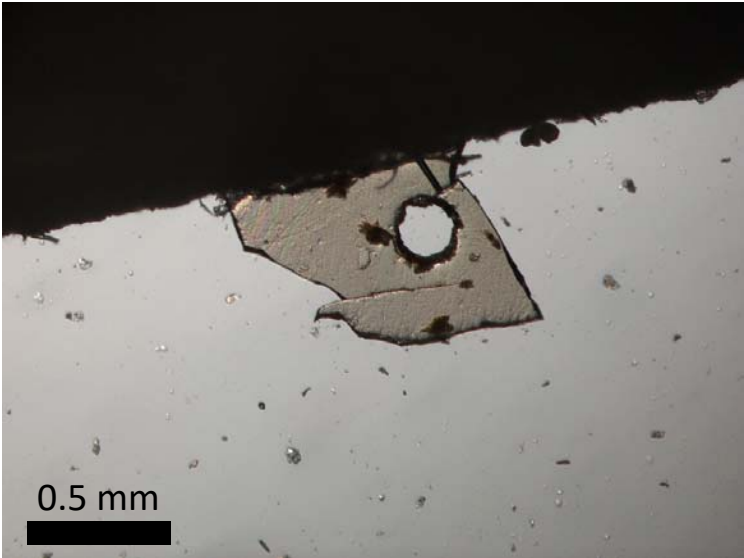


CY16-glass184

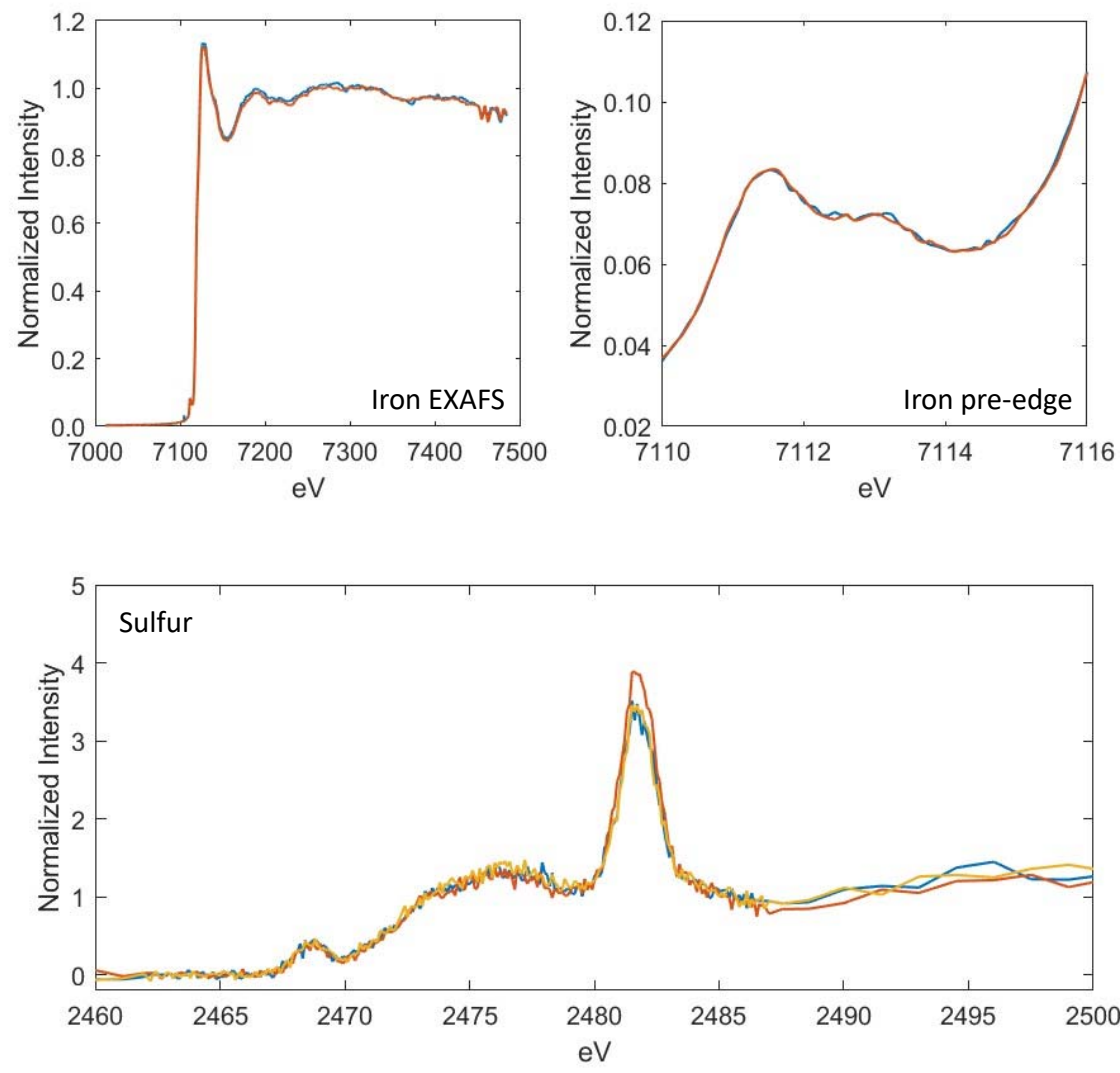
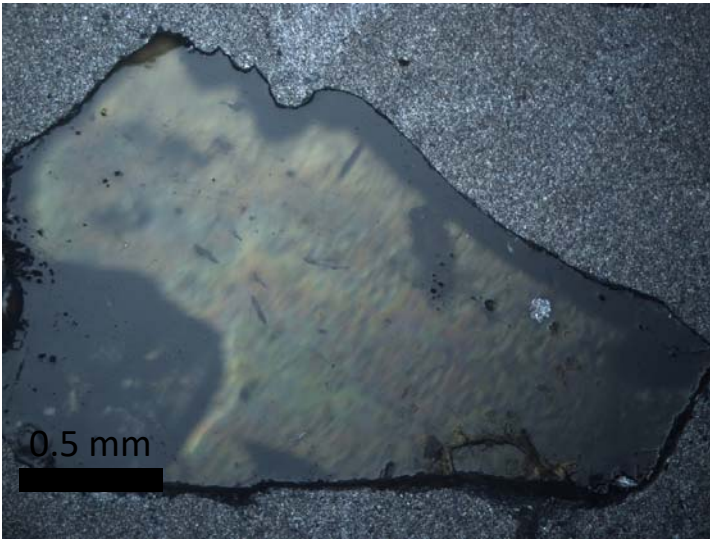




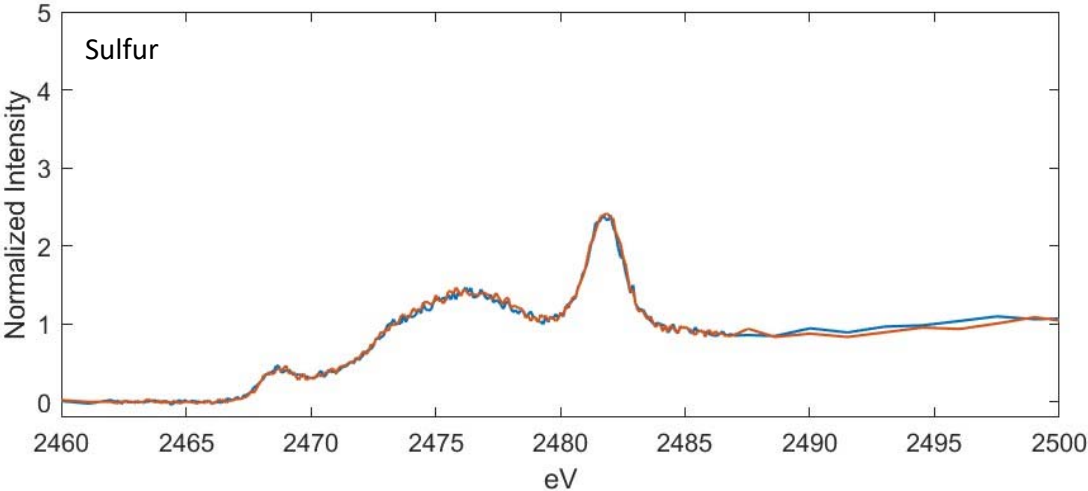
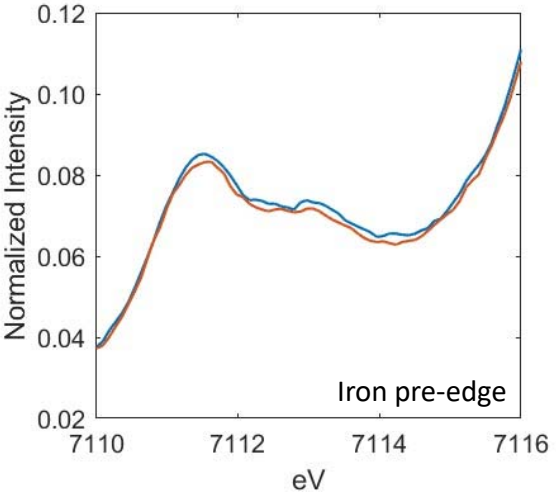
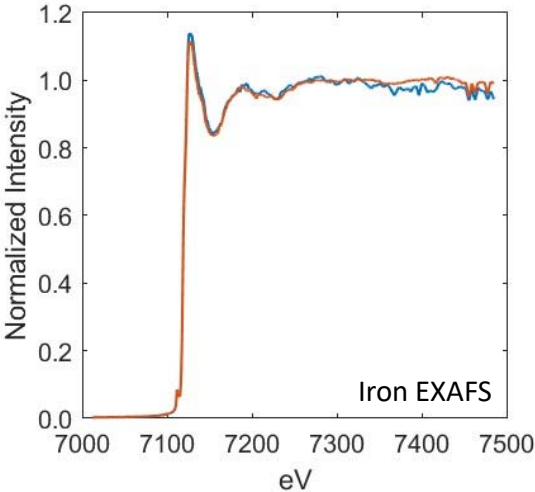
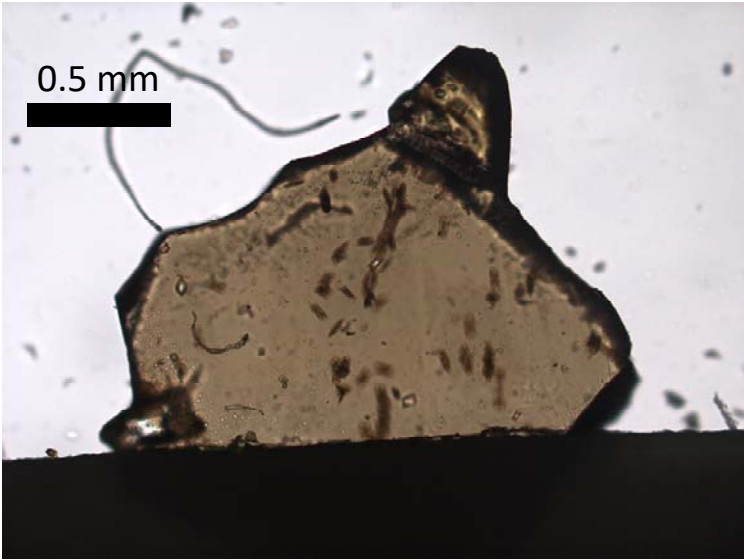
CY16-PK-7



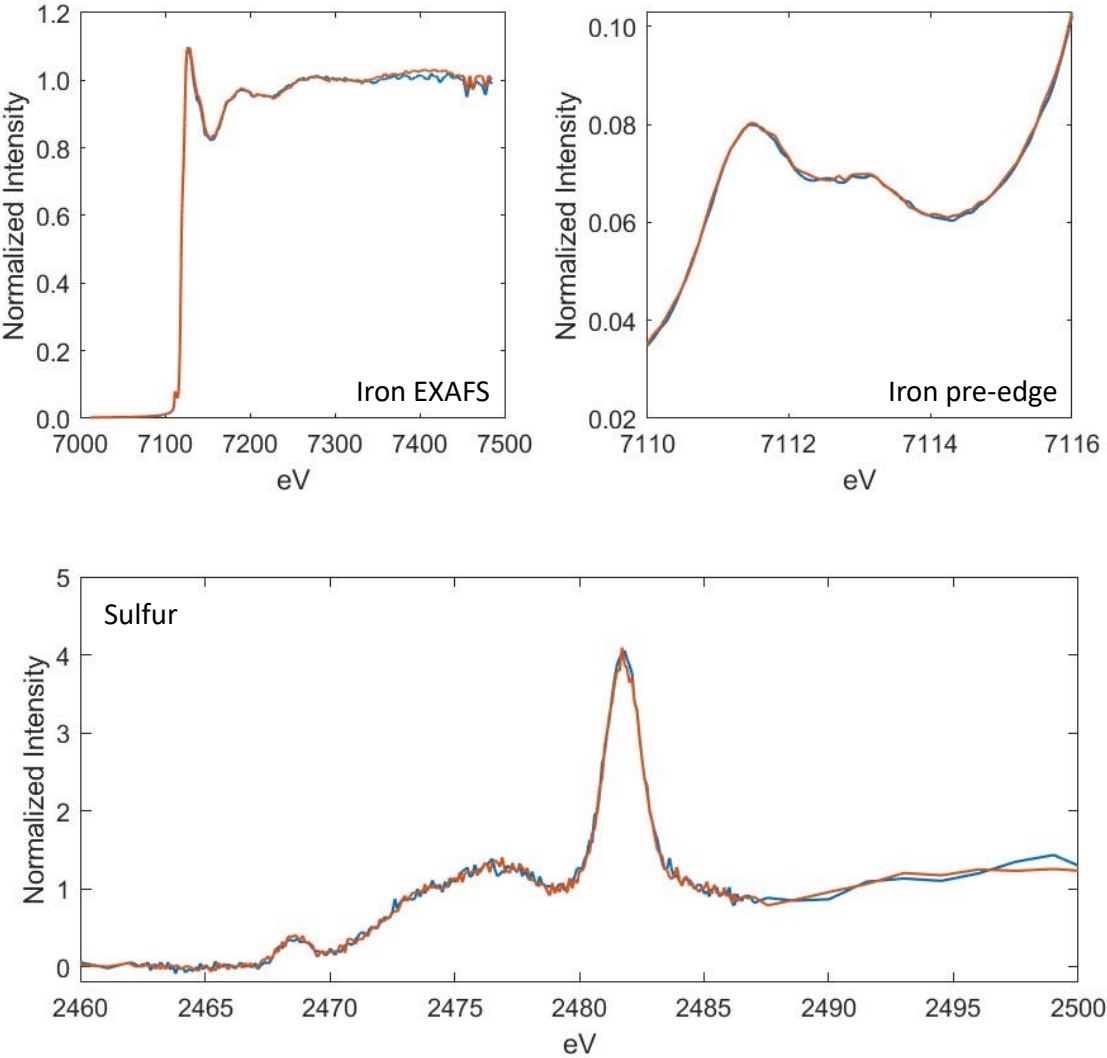
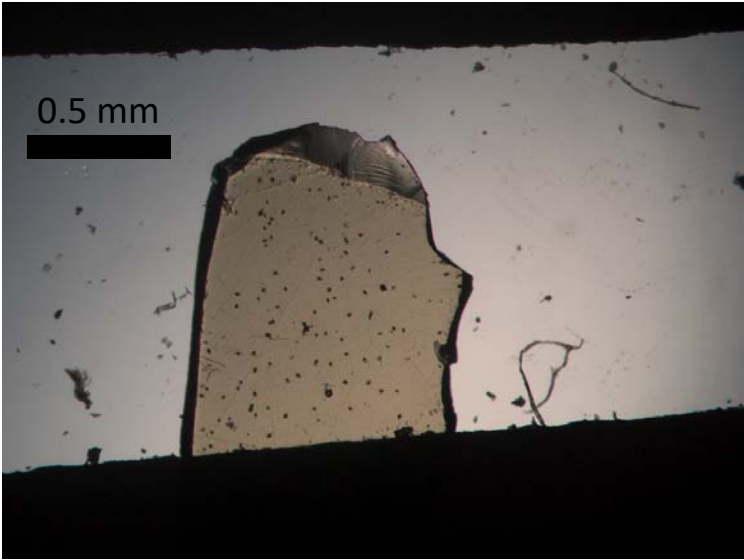
CY16-AK-7



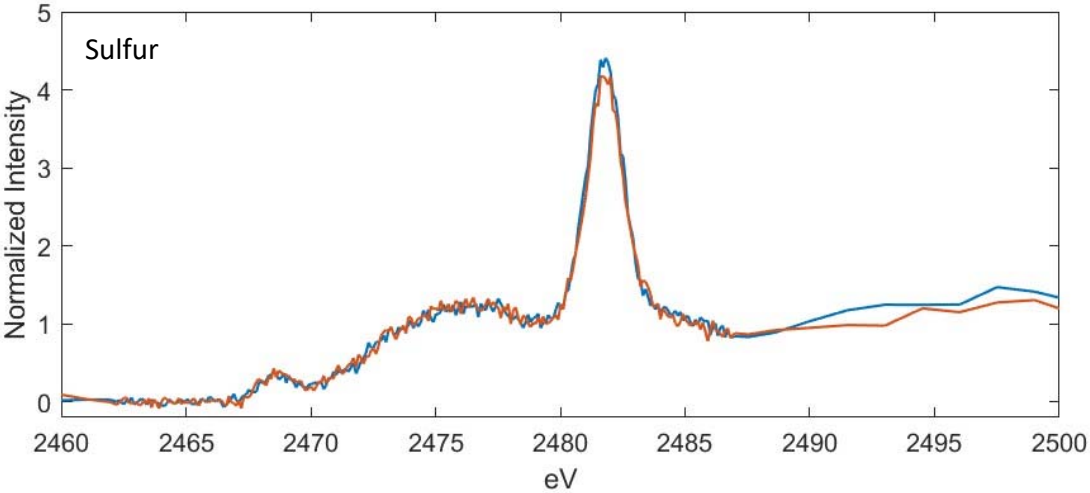
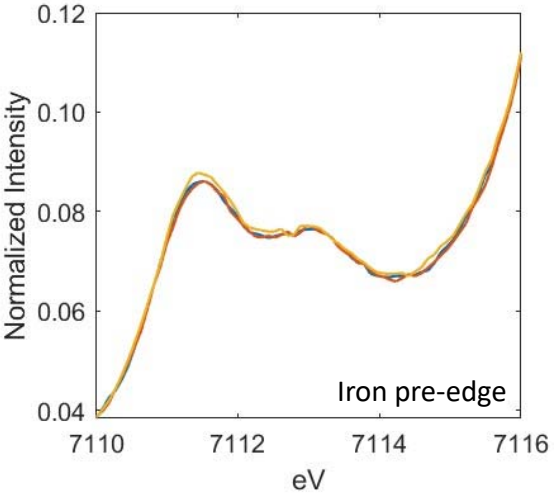
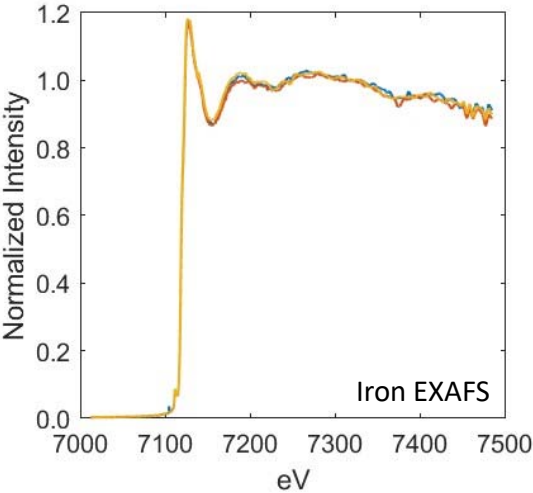
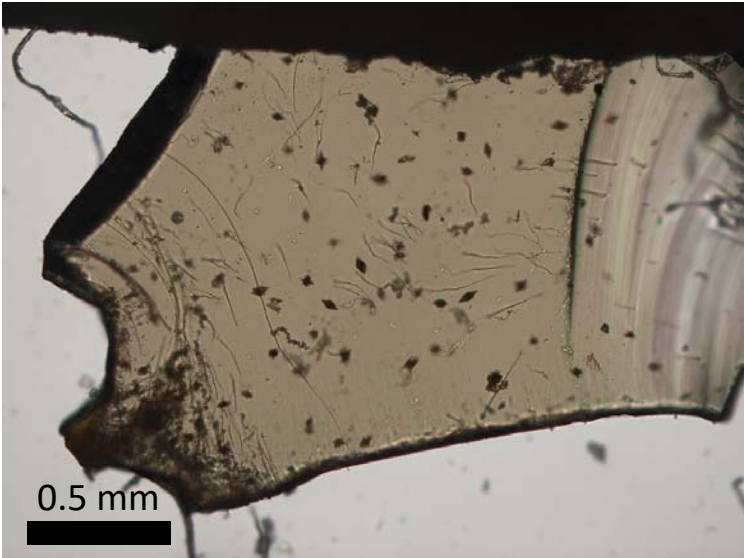
CY16-PK-21



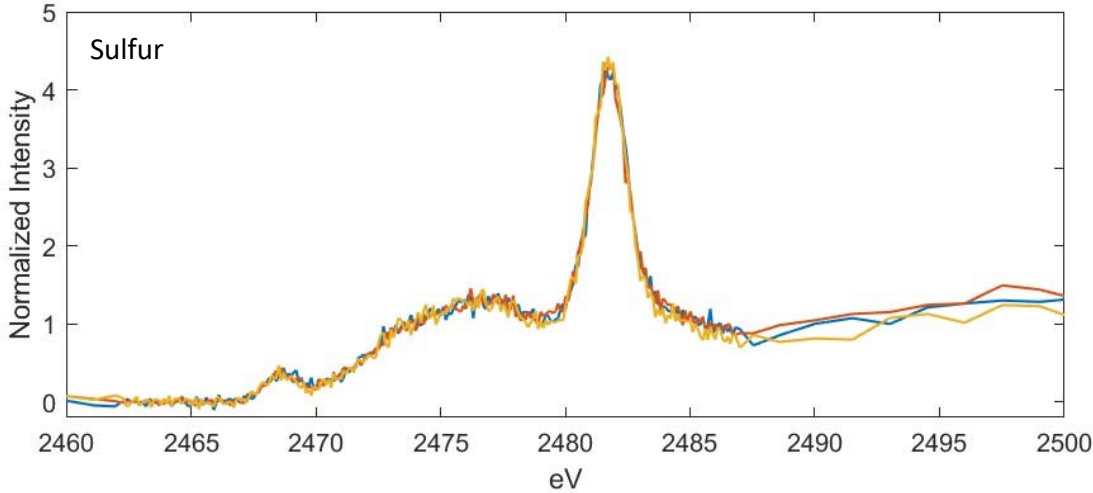
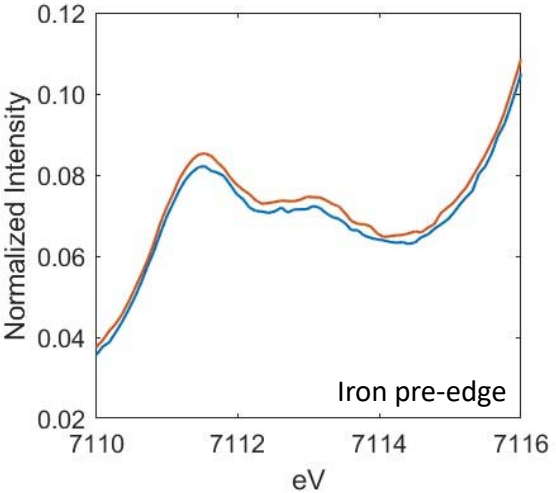
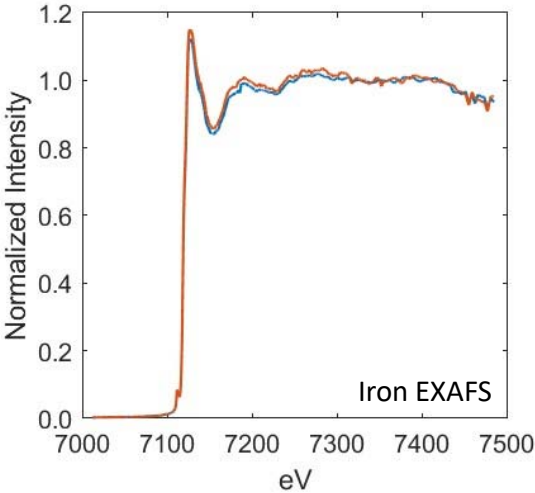
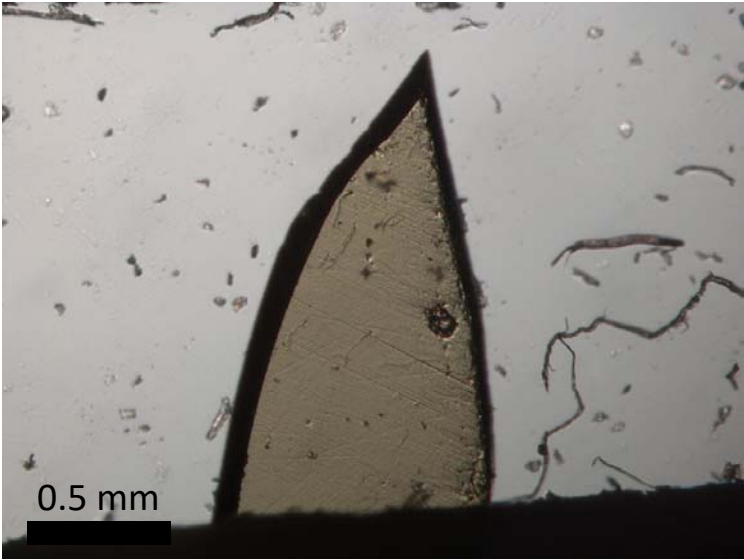
CY17-KV-11



CY17-KV-14

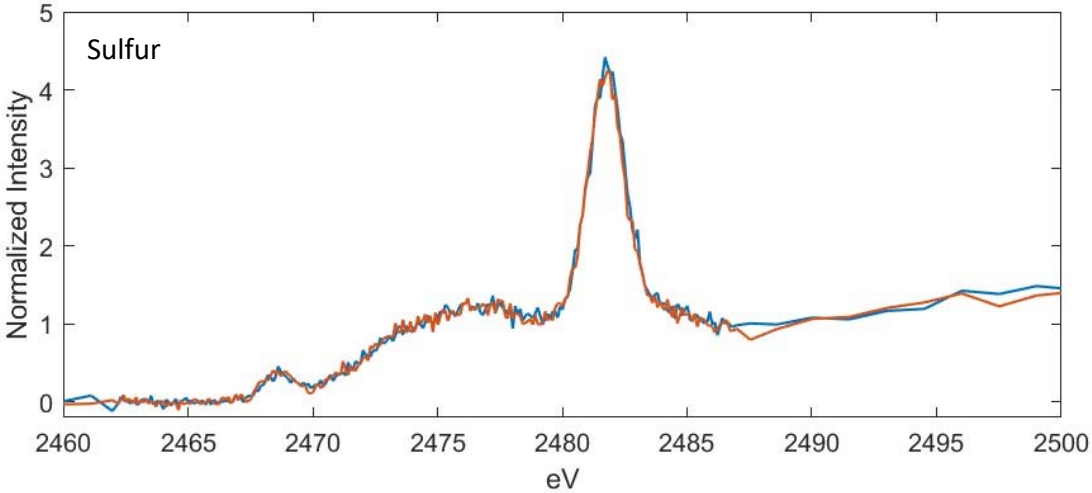
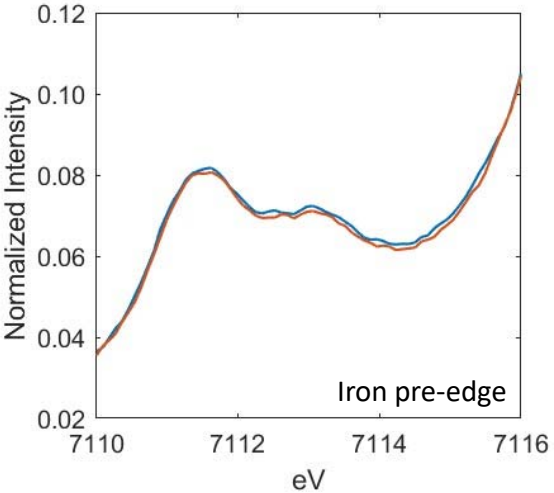
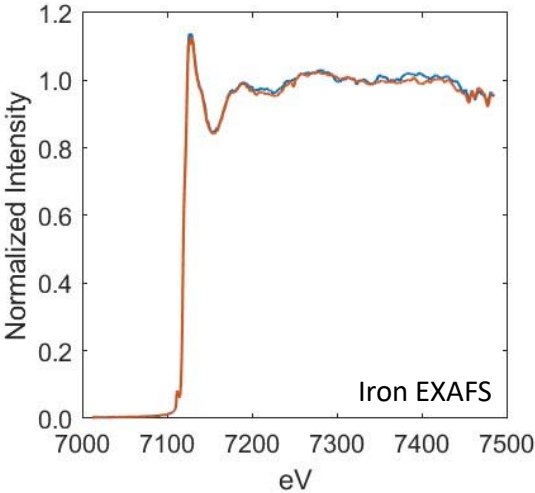
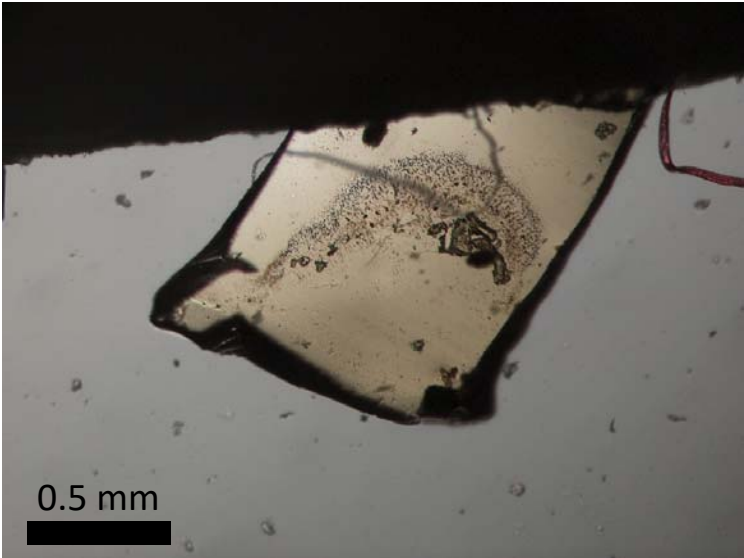


CY17-KV-39

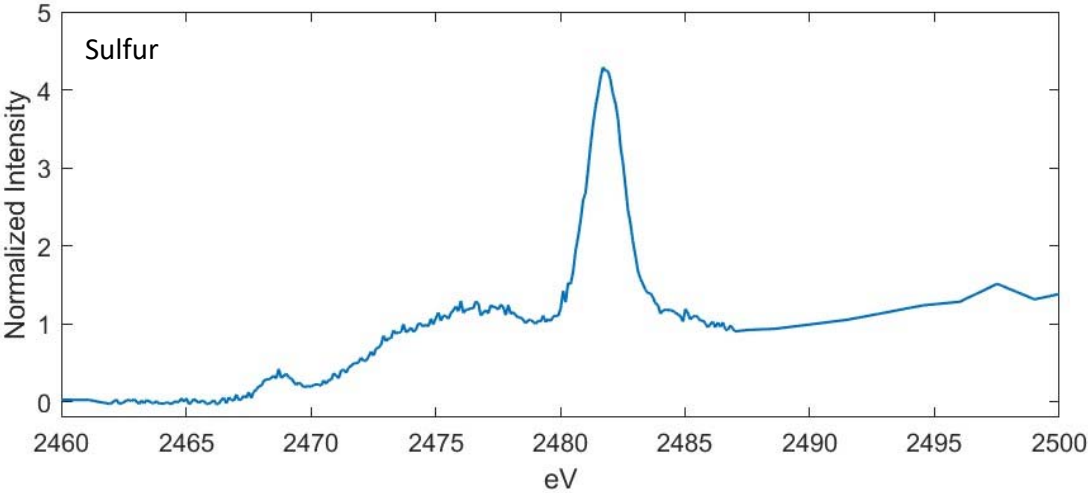
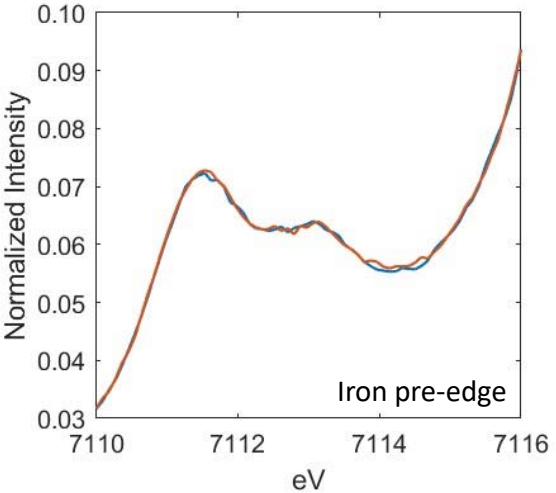
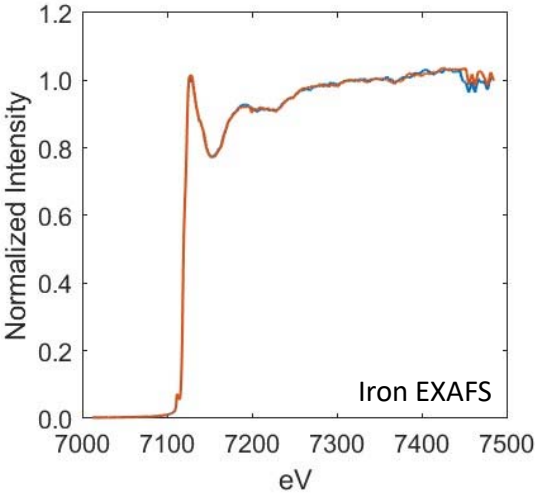
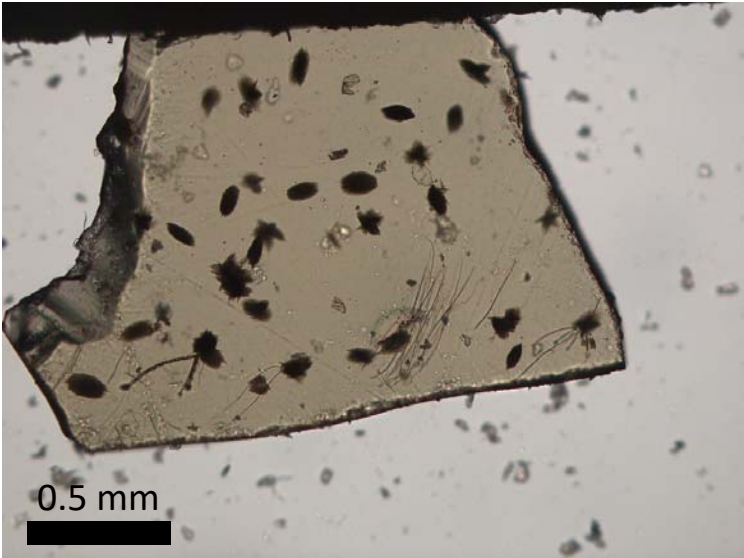




CY17-KV-44



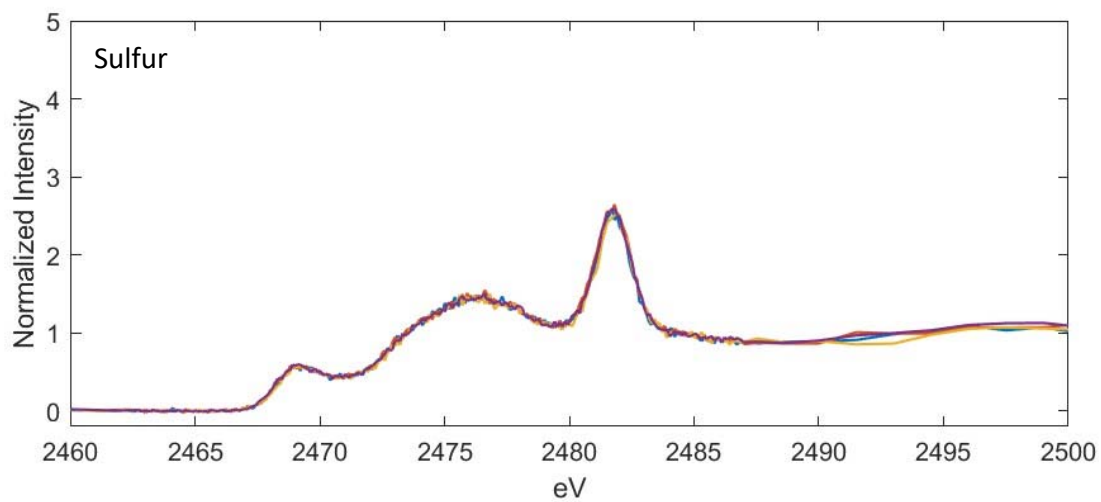
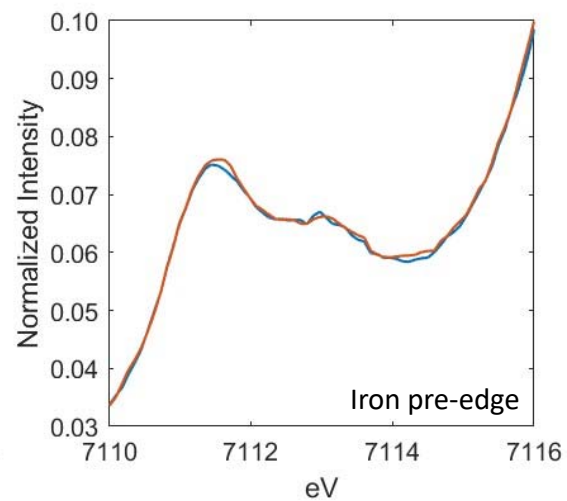
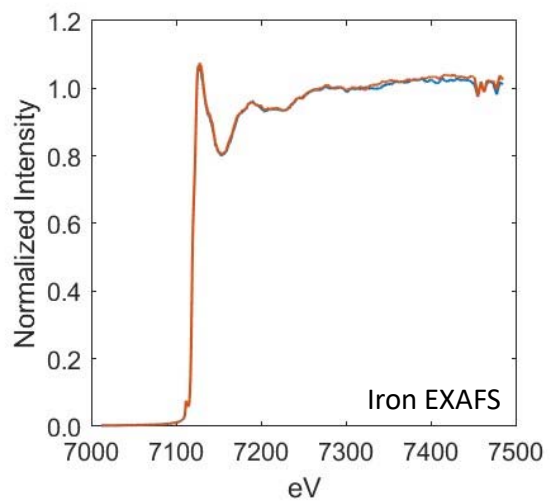
CY17-KV-48



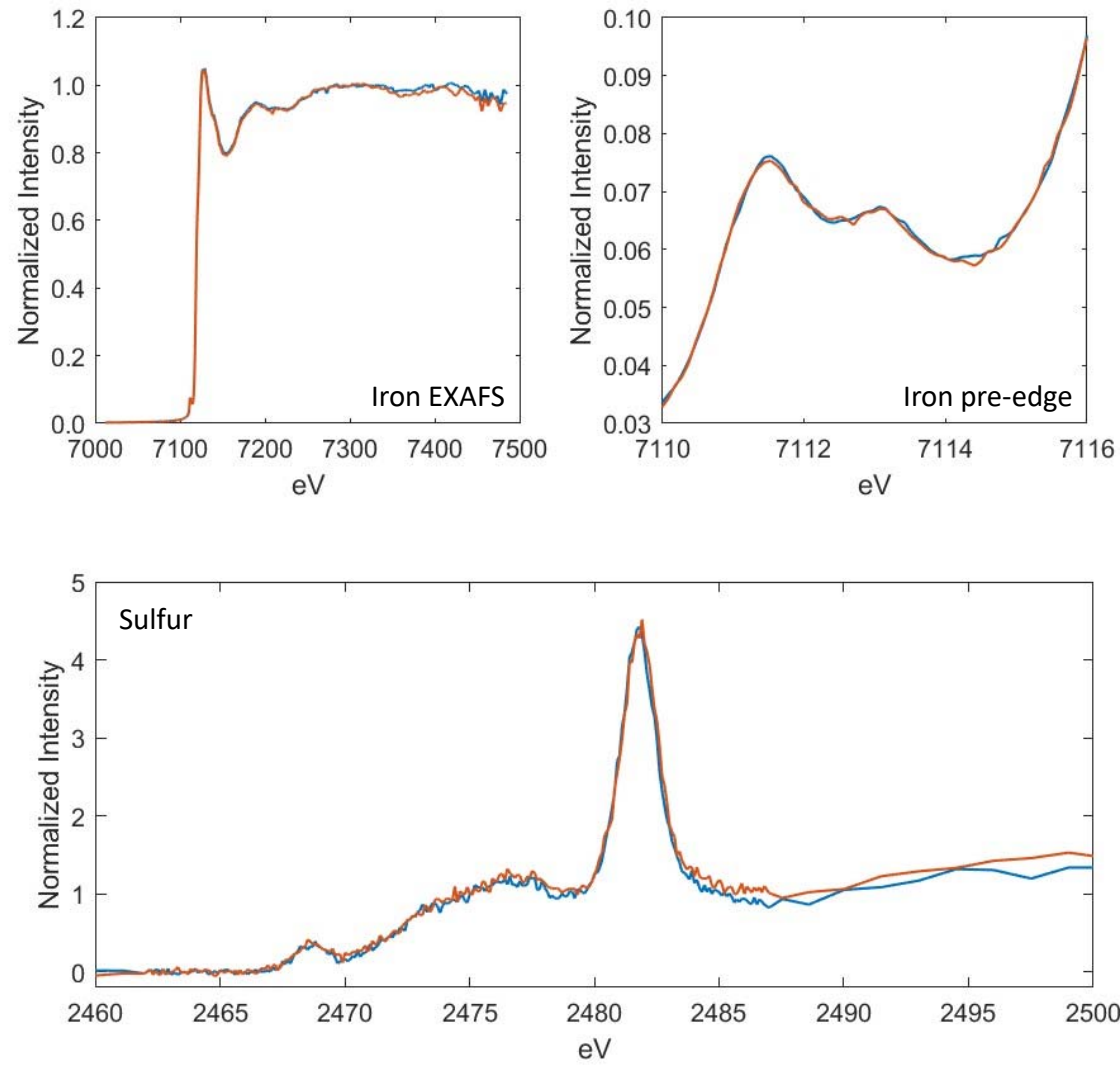
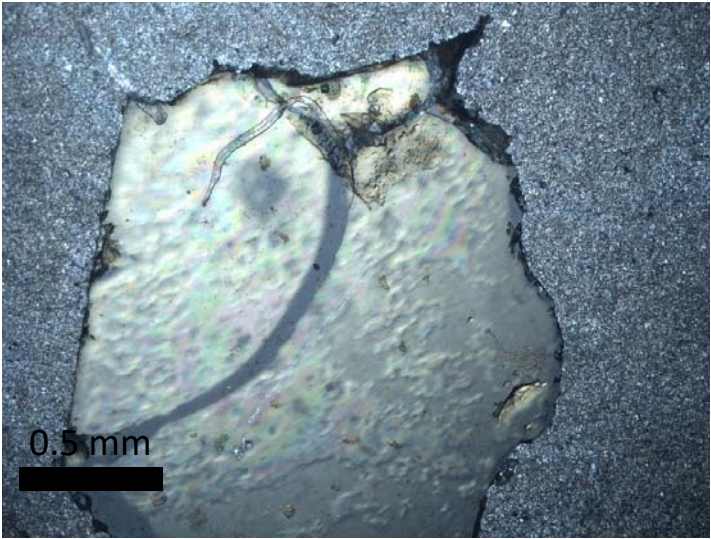


CY17-KV-50

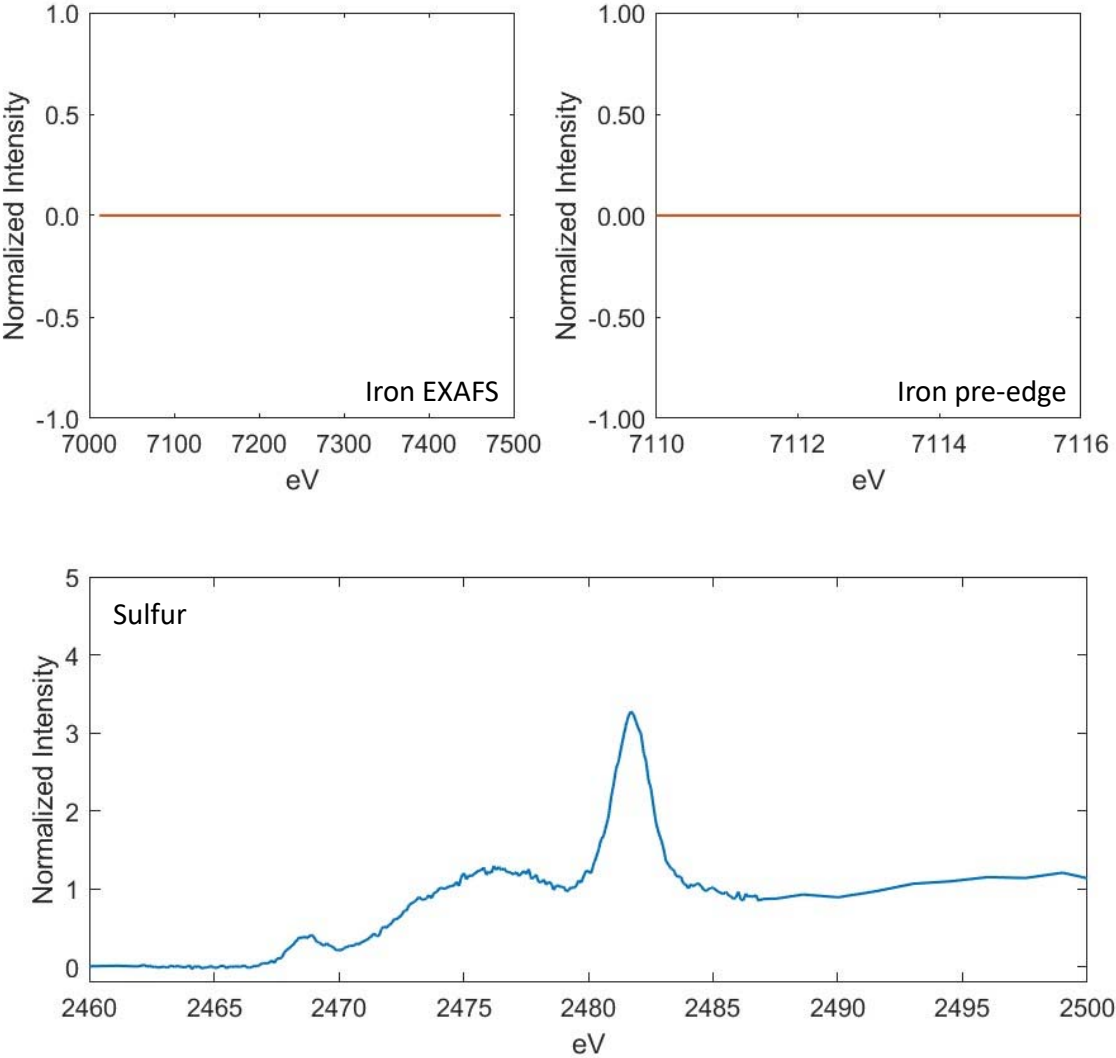
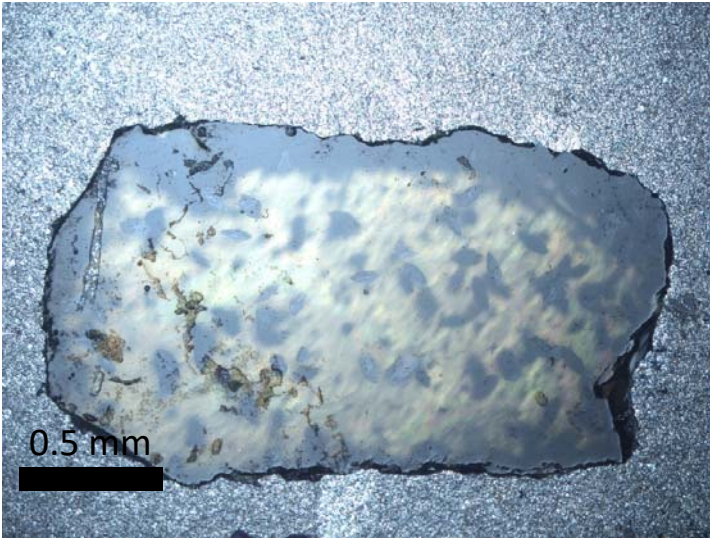
0.5 mm



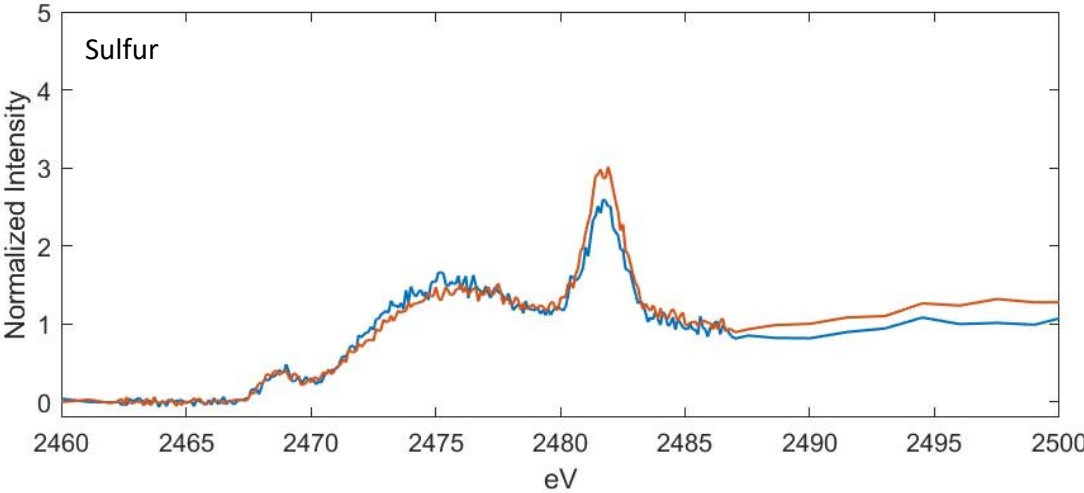
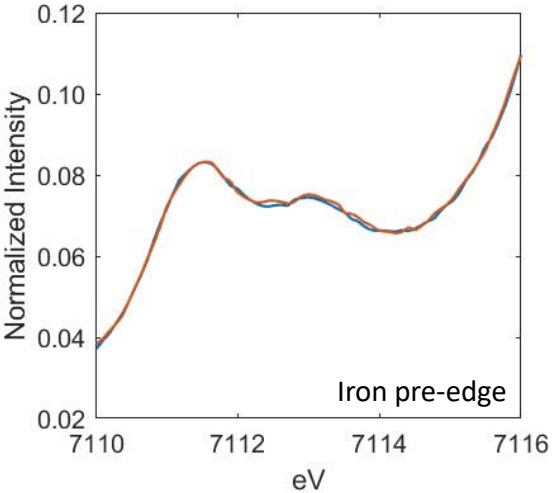
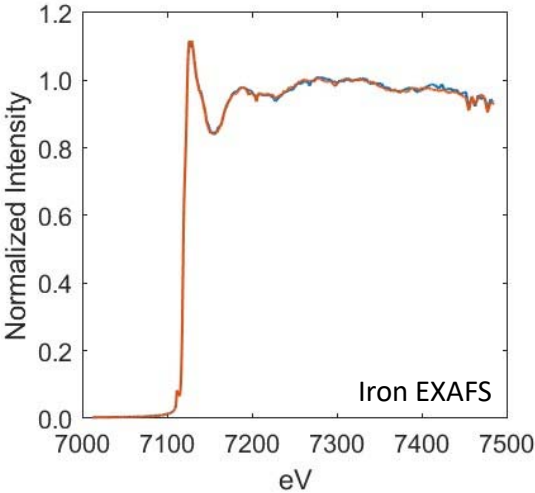
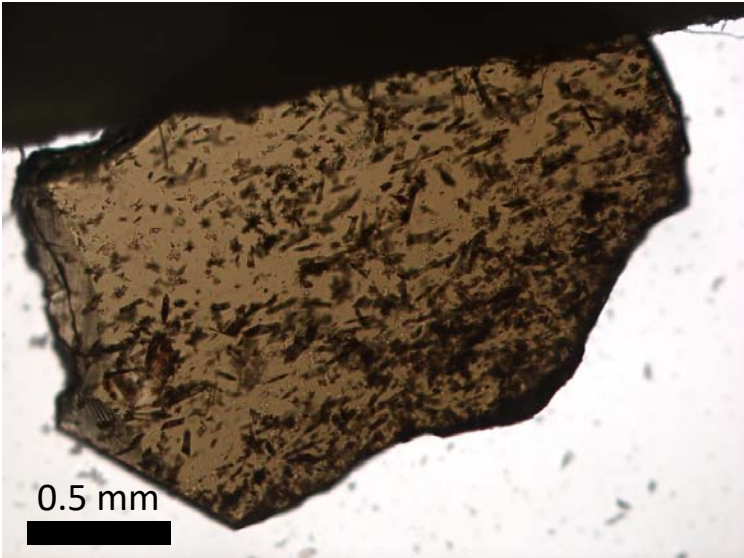
CY17-KV-51



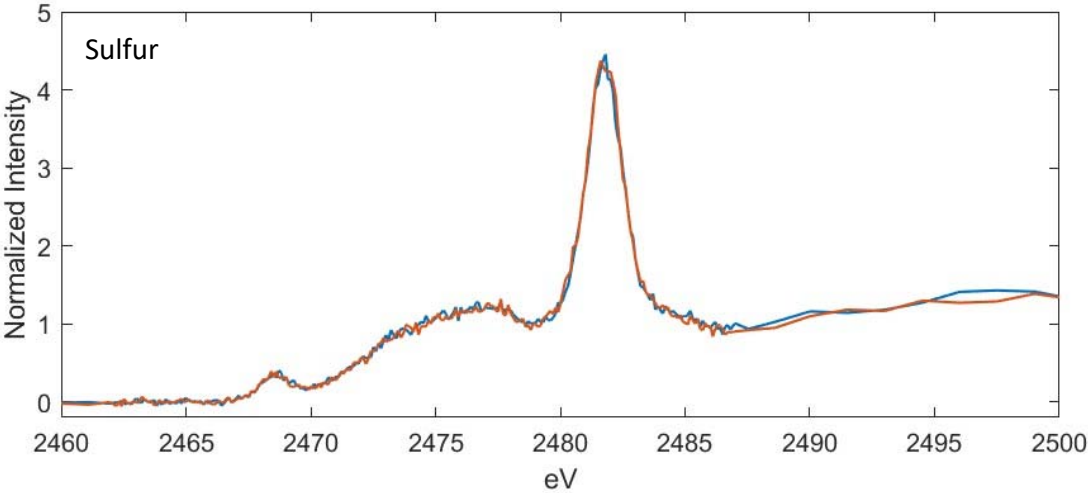
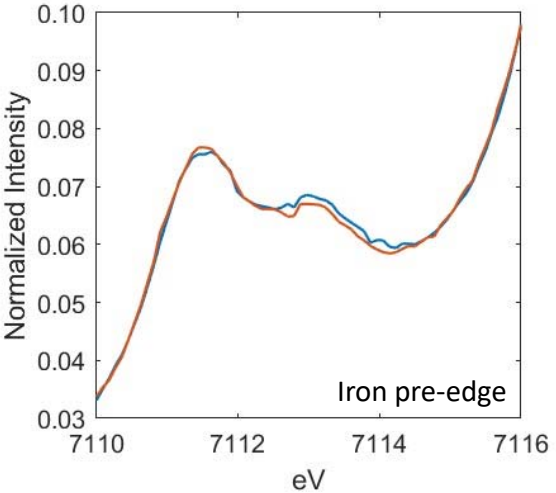
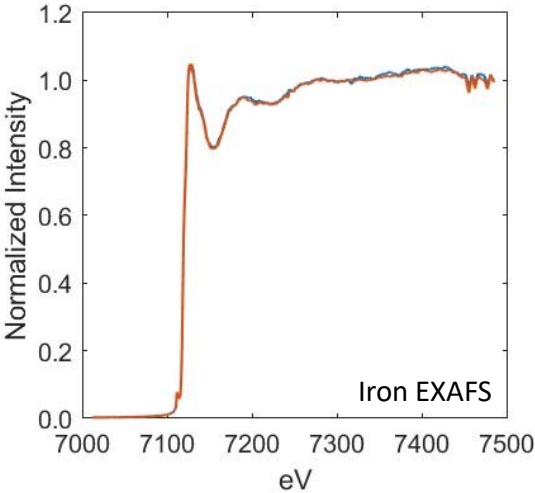
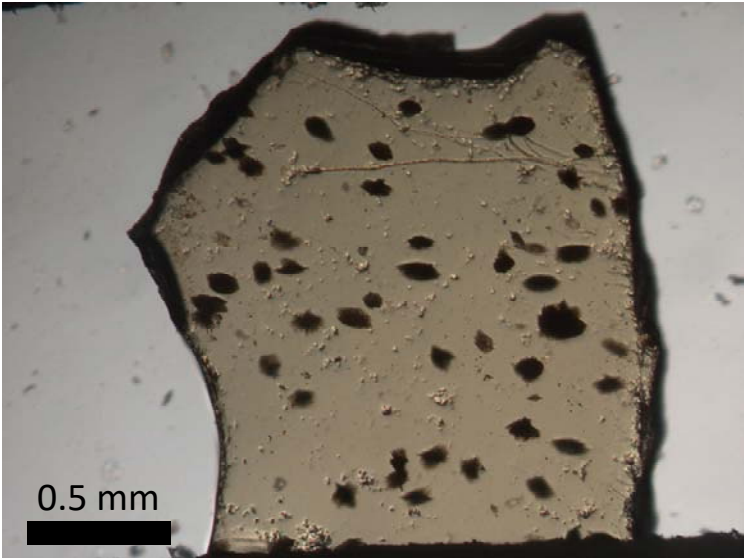
CY17-KV-53



CY17-KV-56

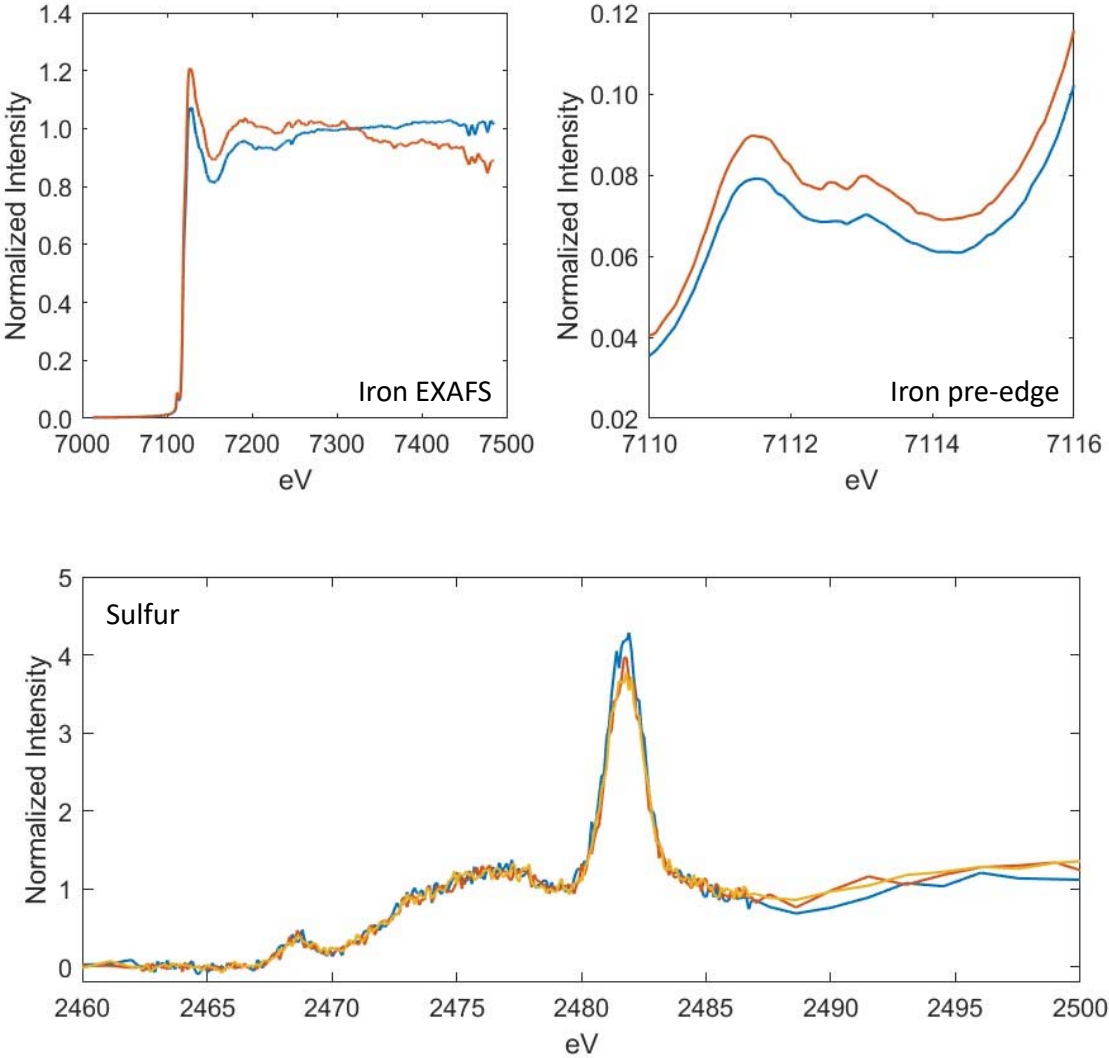
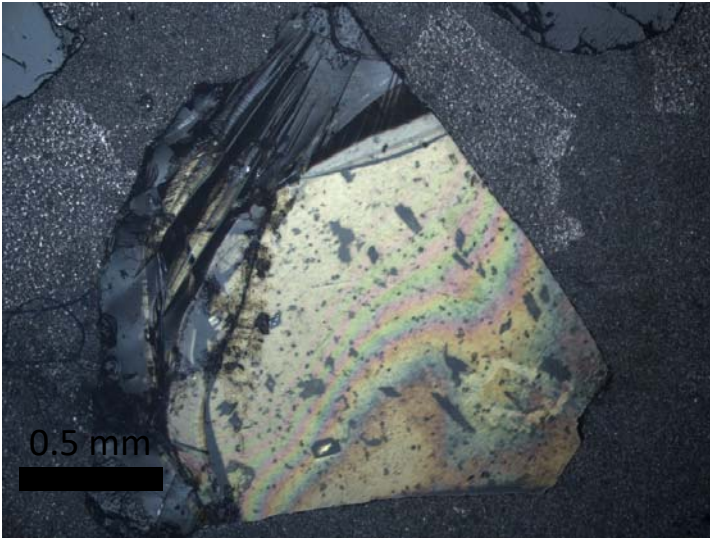


CY17-KV-79

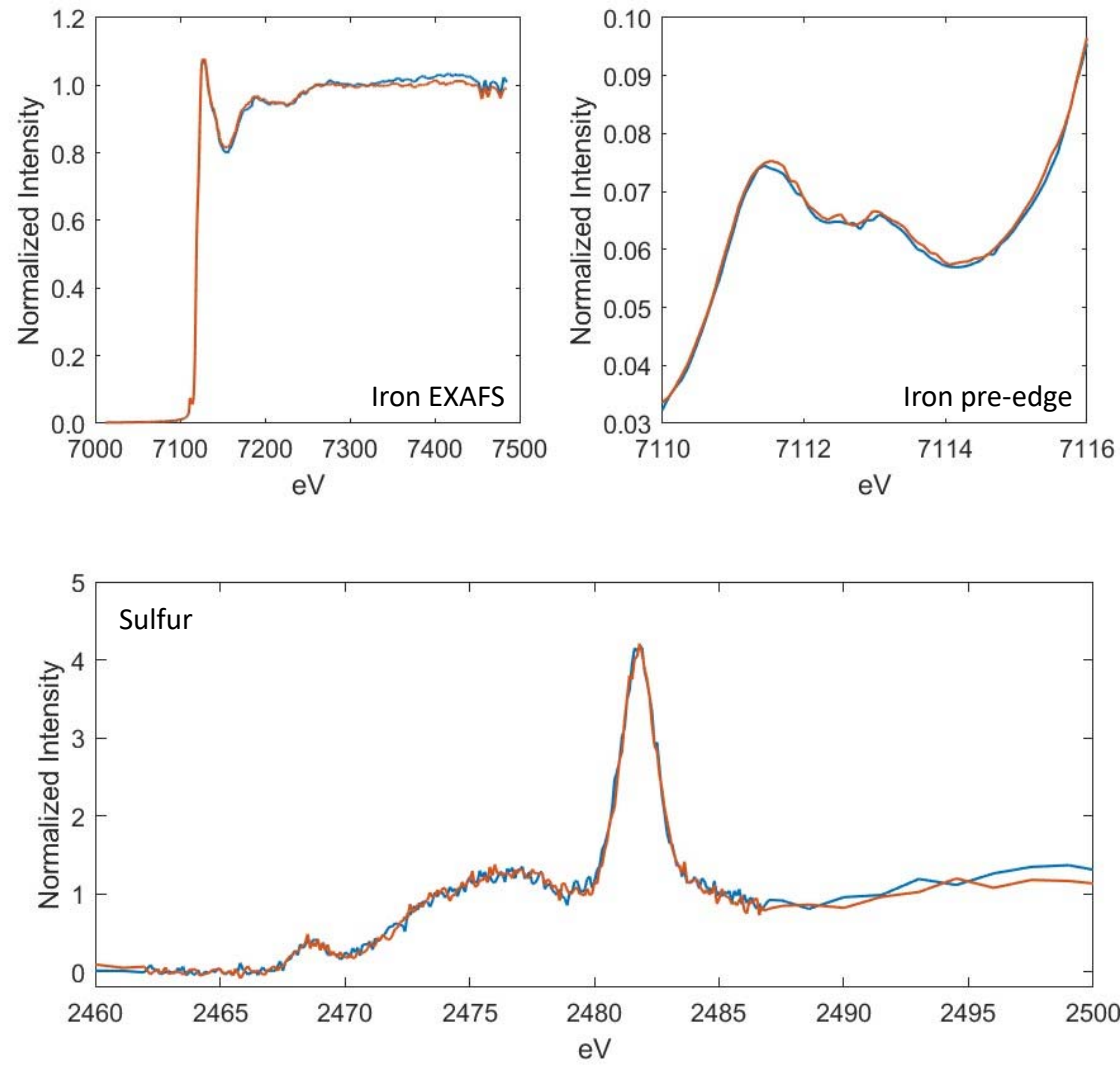
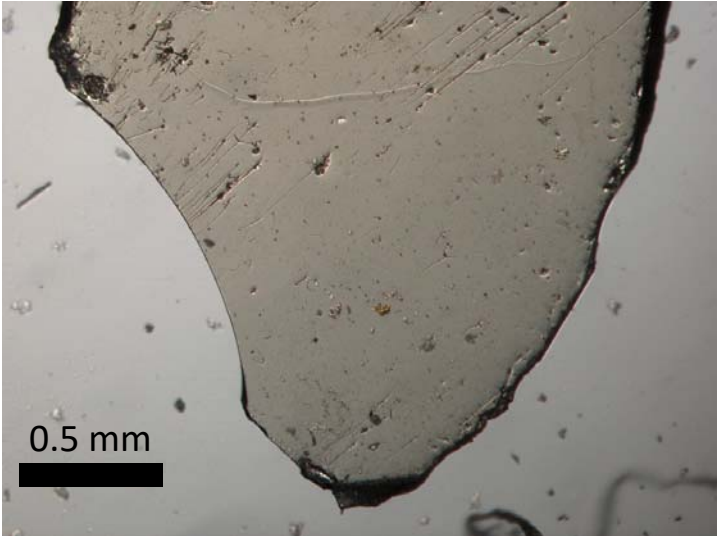




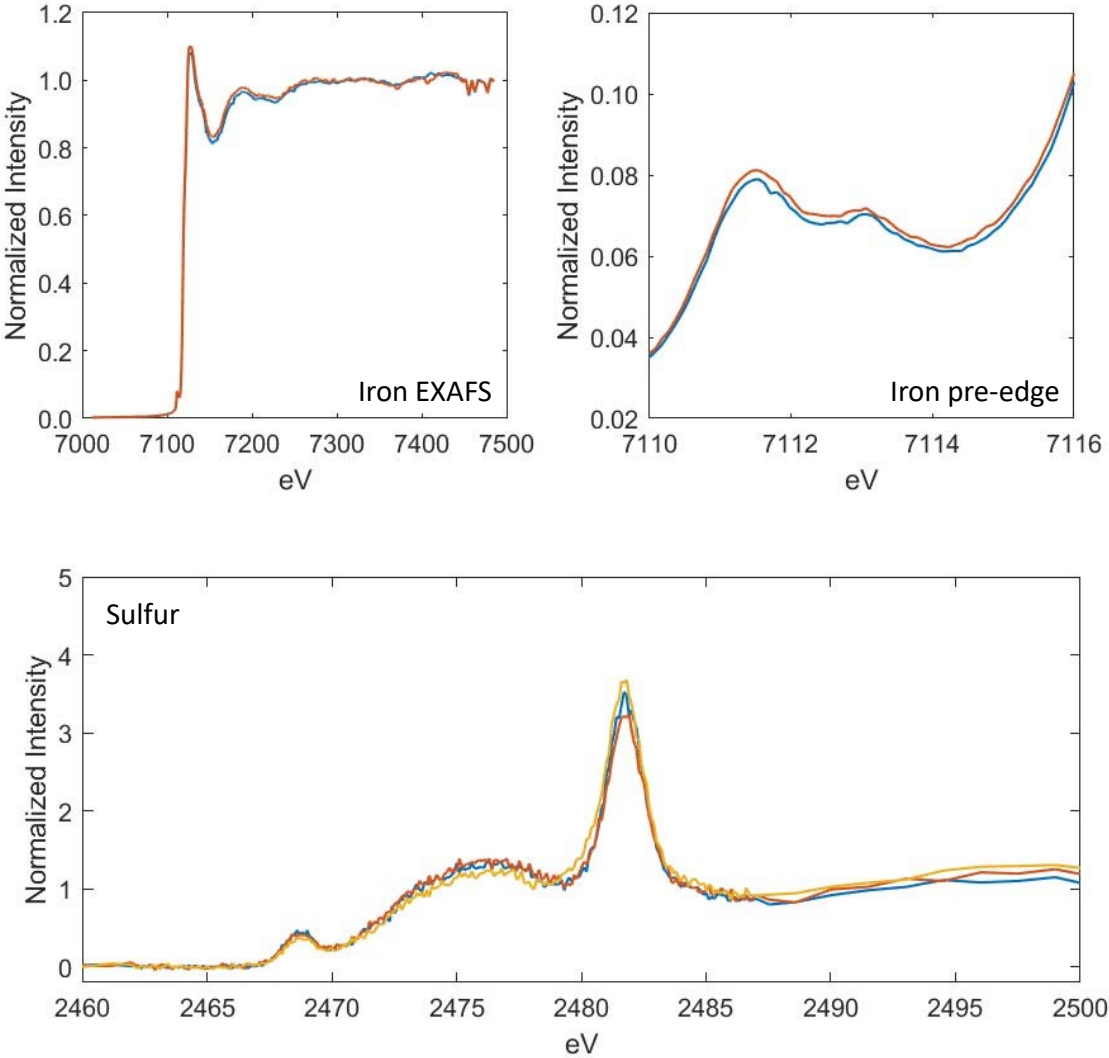
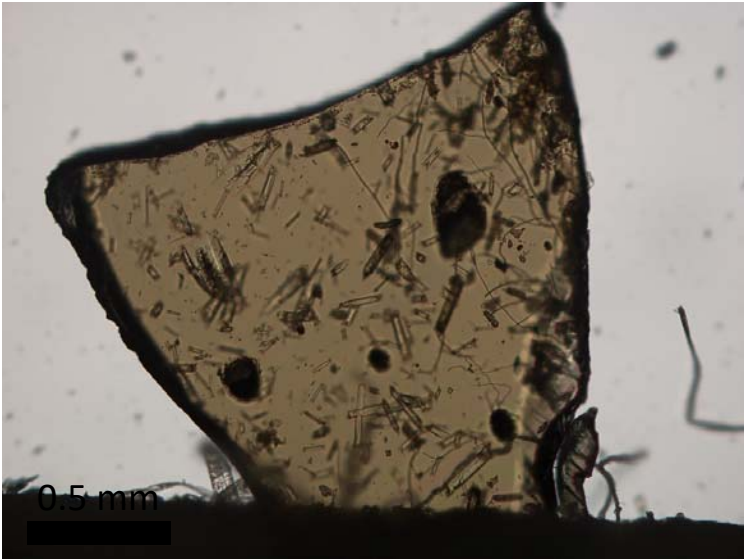
CY17-KV-104



CY17-KV-113

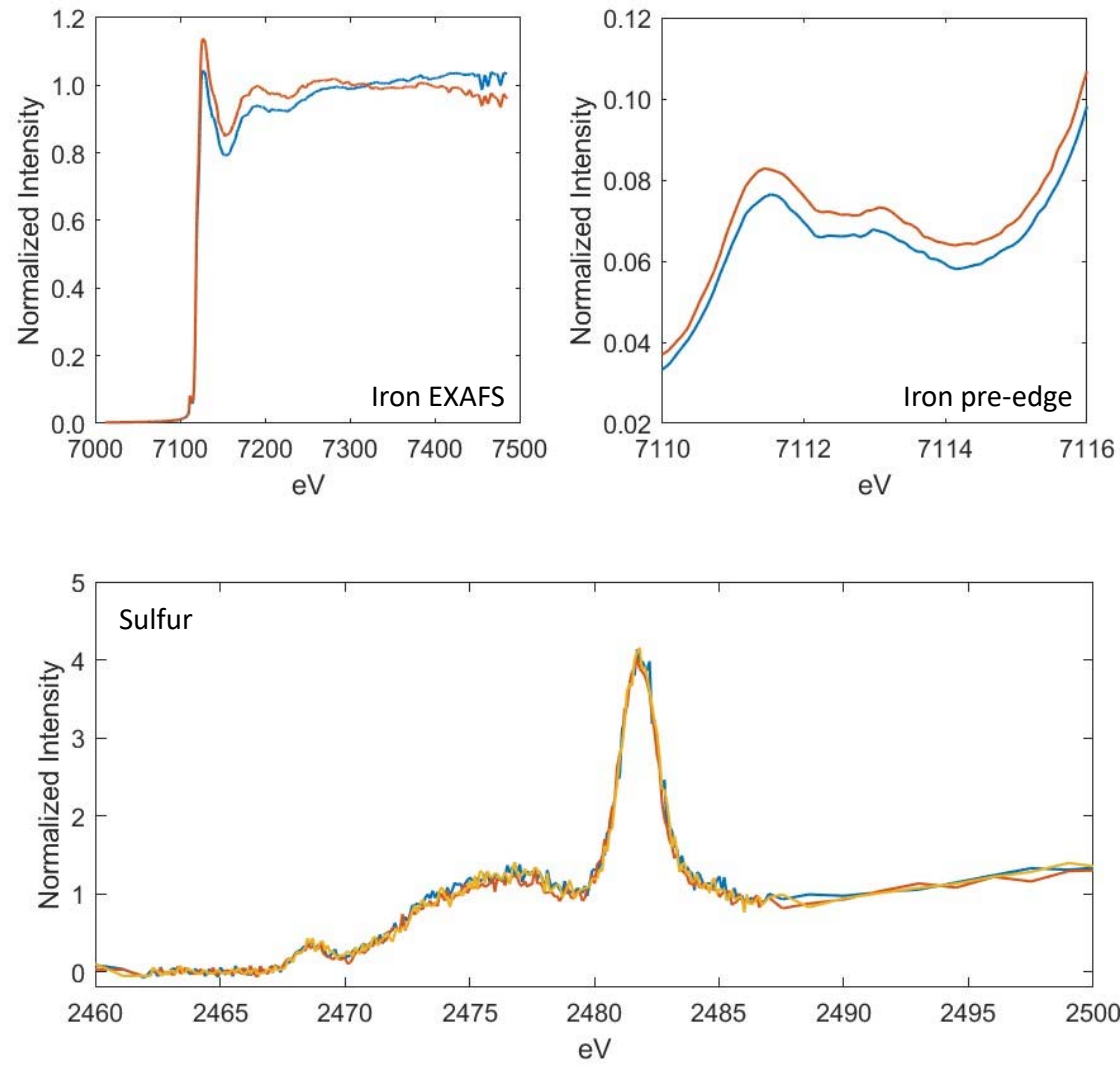
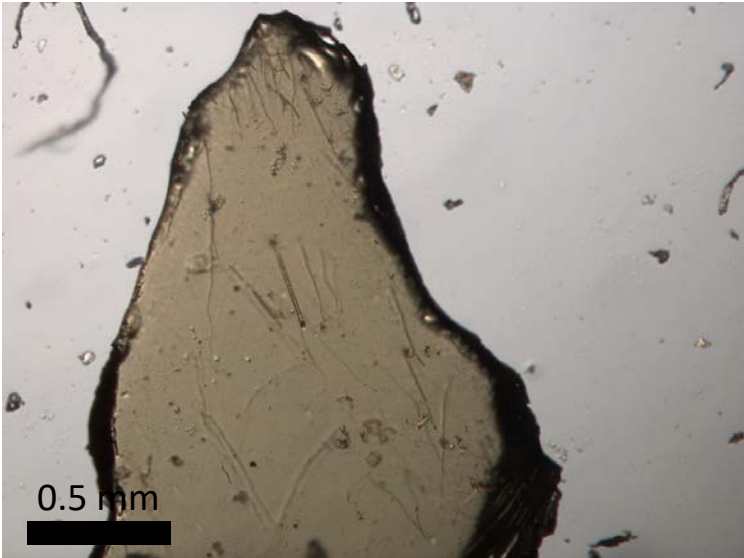


CY18-AR-13

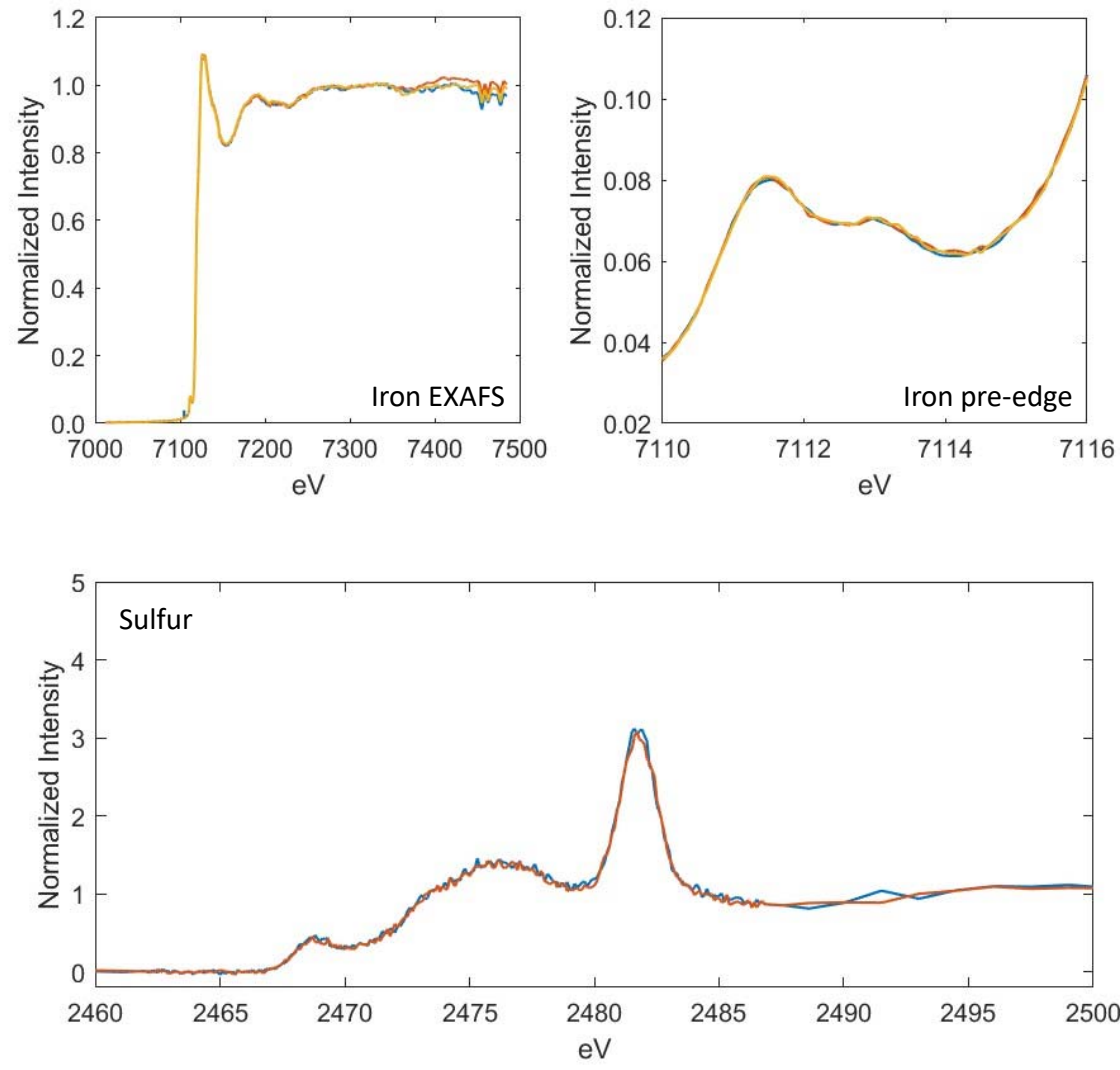
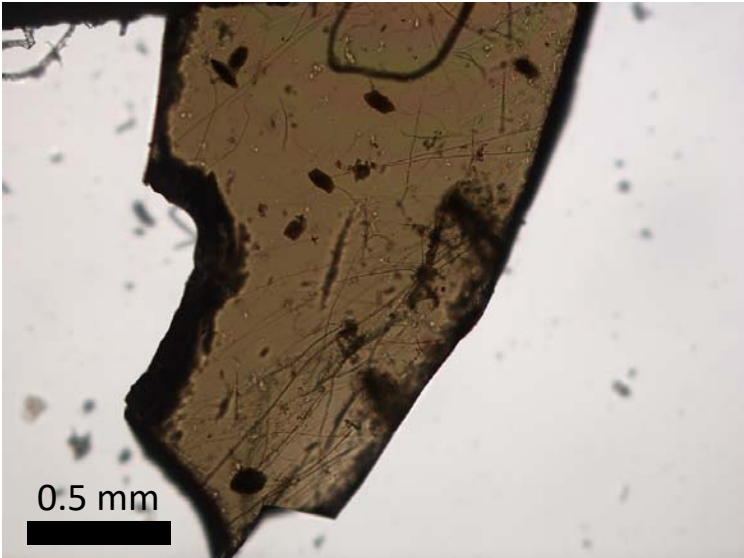




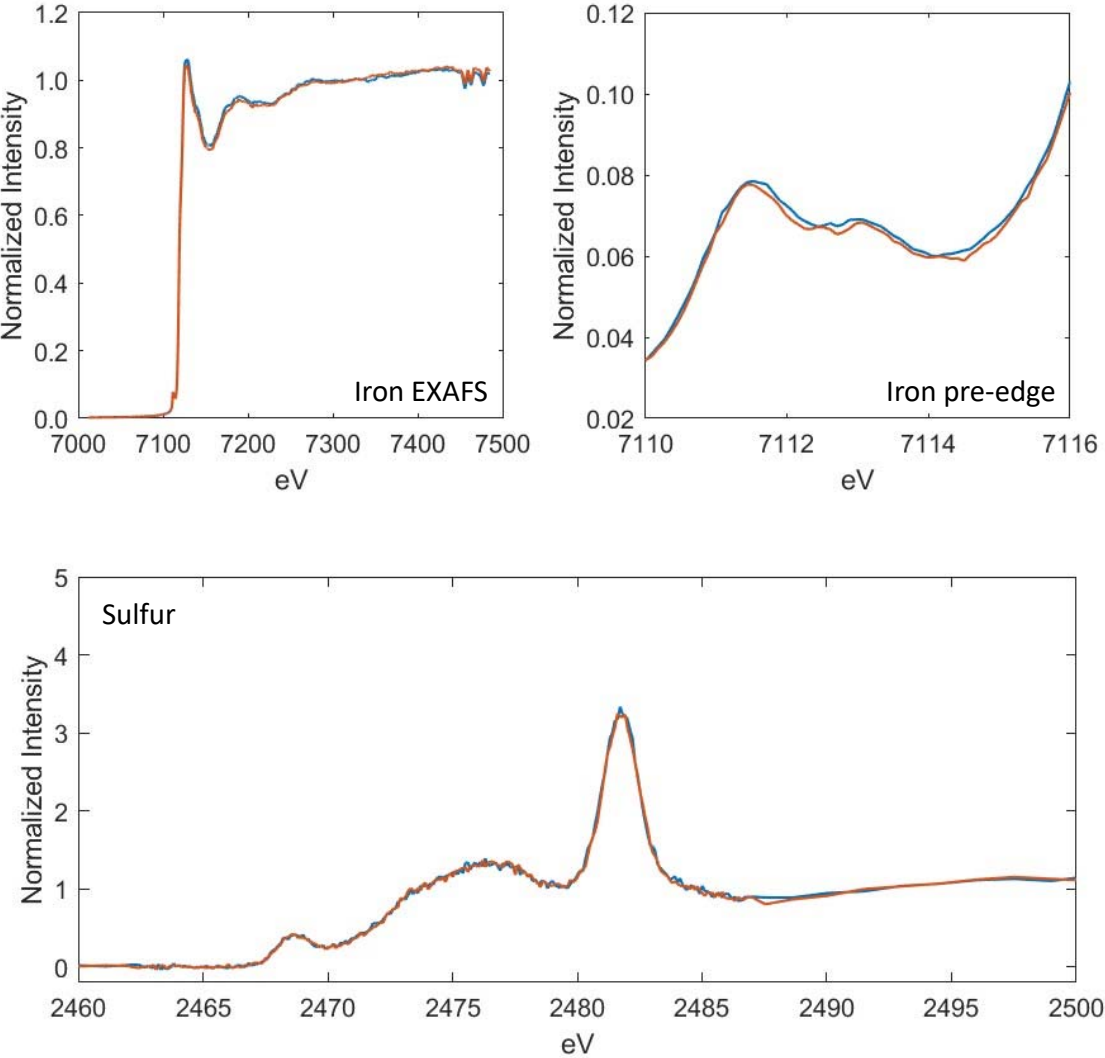
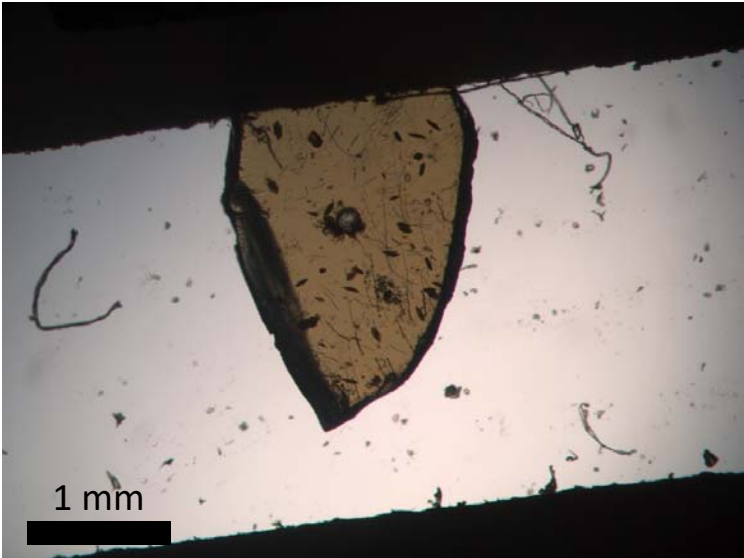
CY18-AR-15



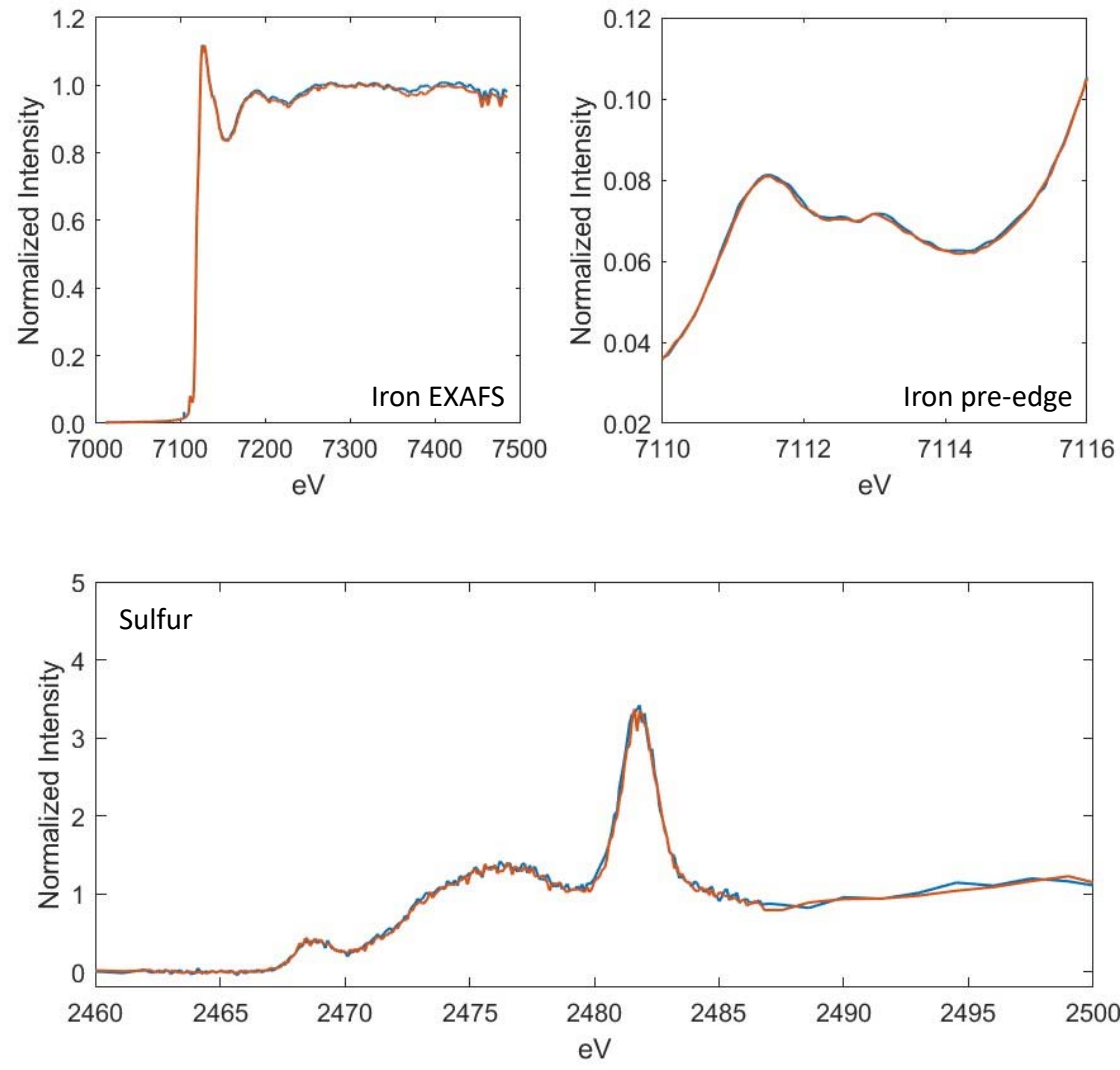
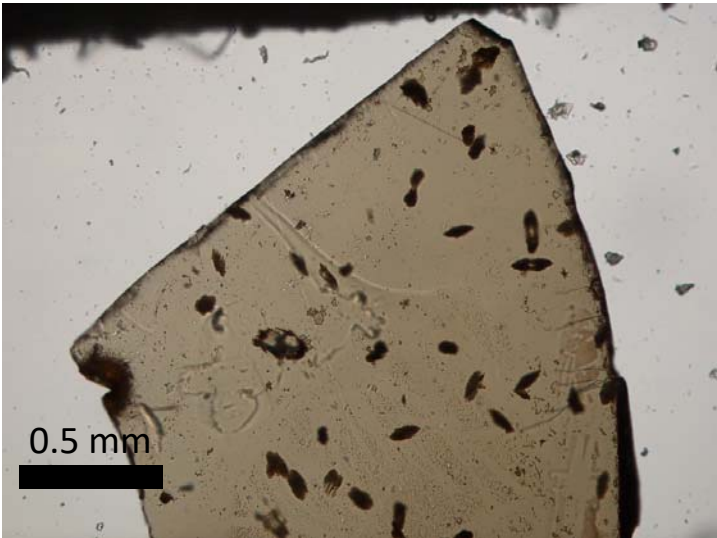
CY18-EA-16



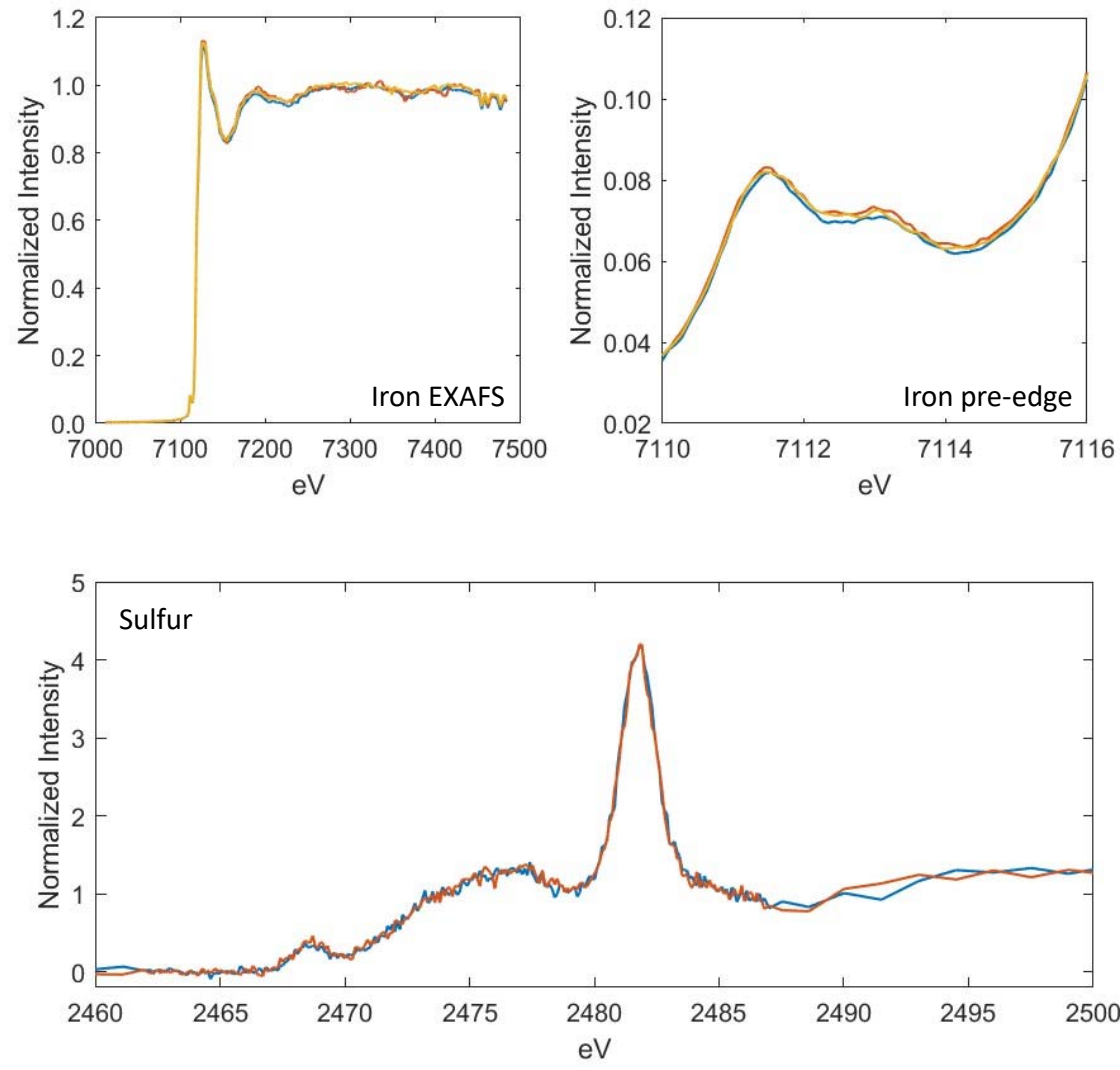
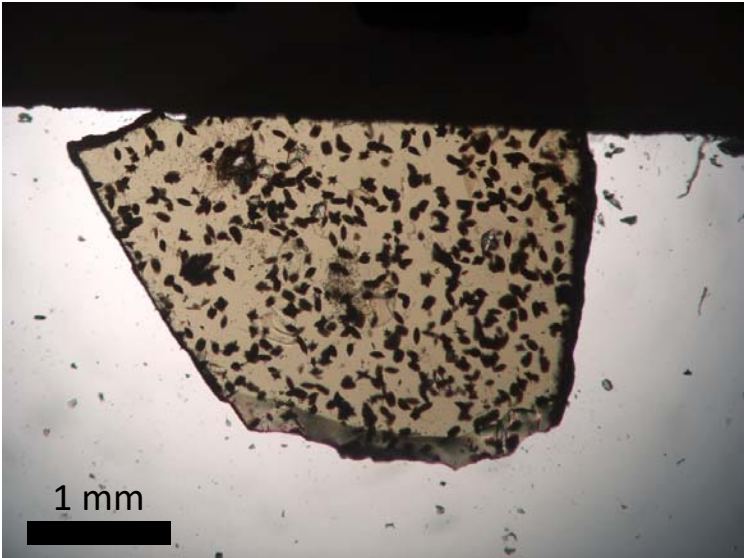
CY18-EA-31



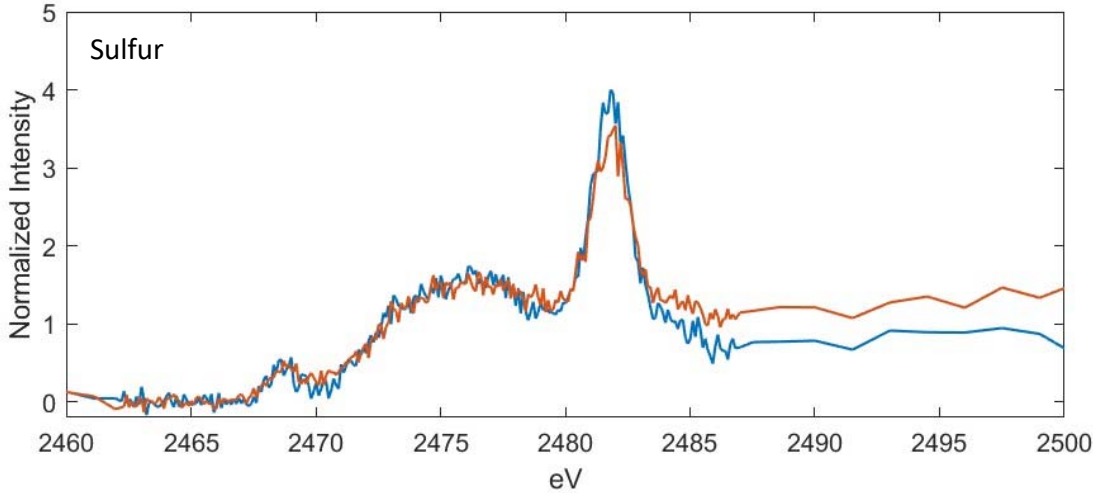
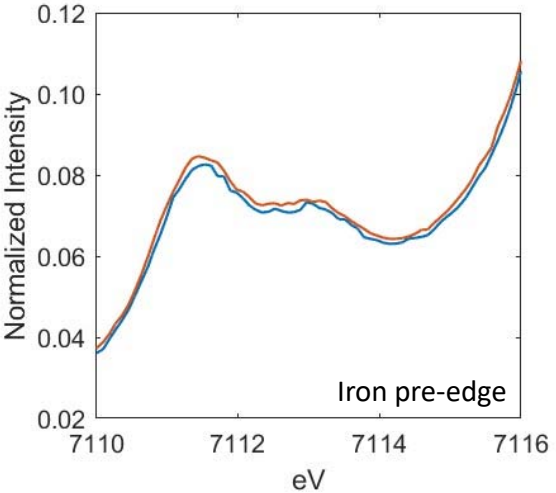
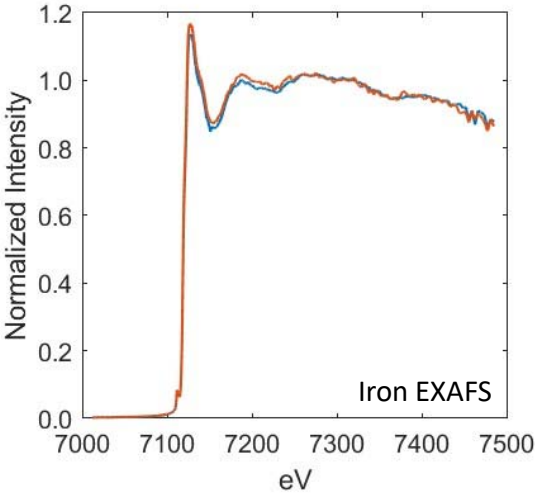
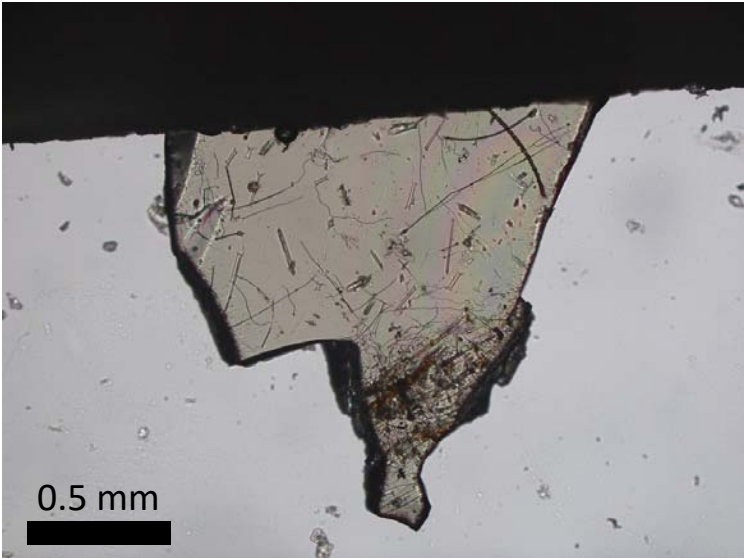
CY18-EA-36



CY18-MA-7

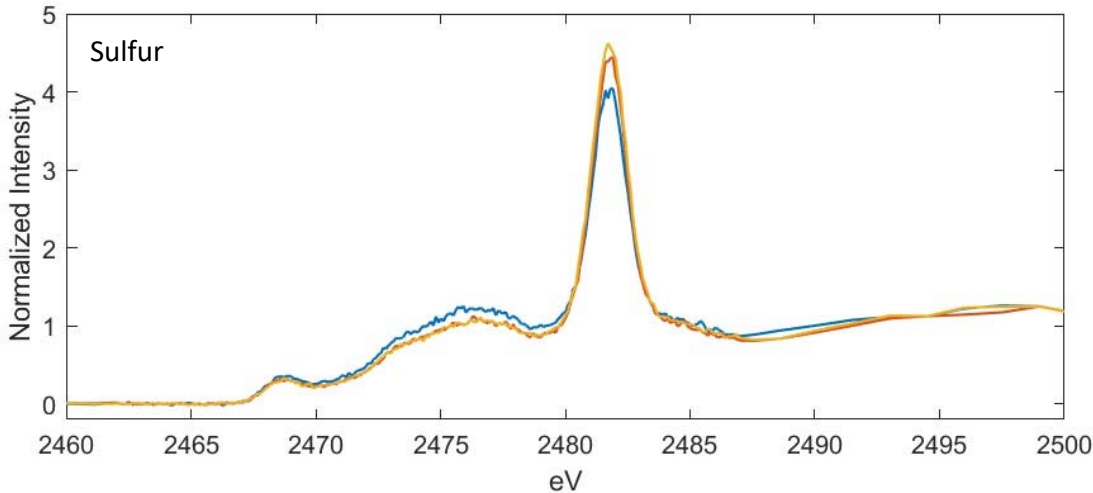
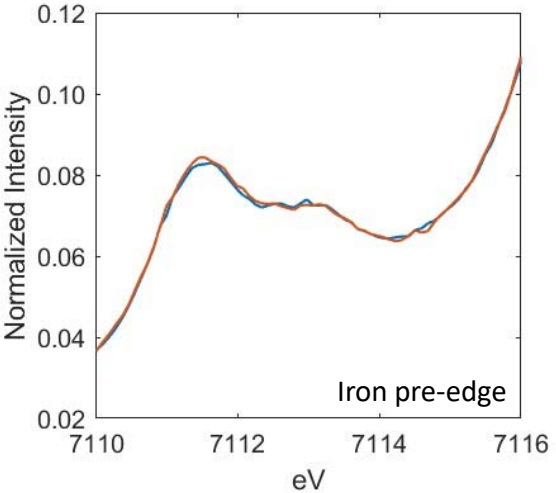
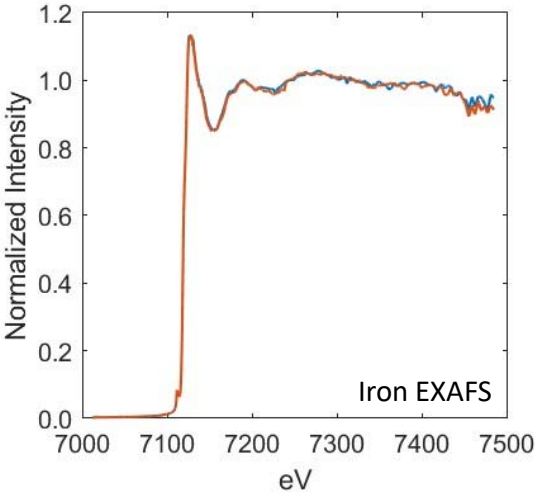
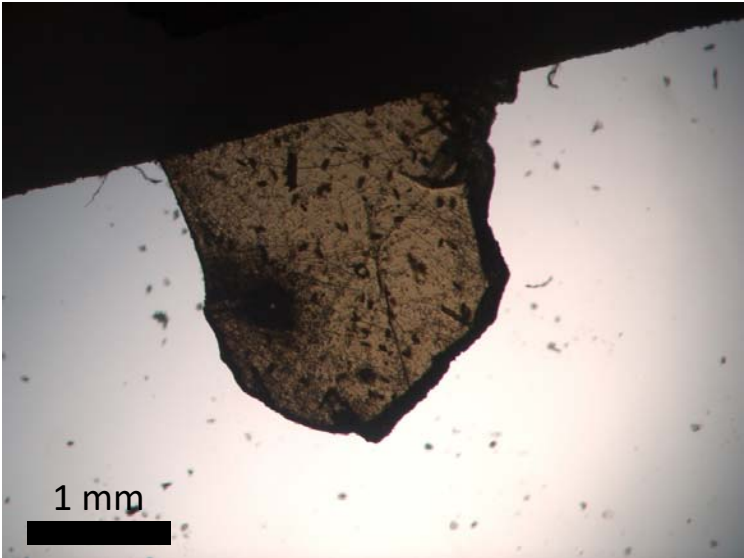


CY16-21

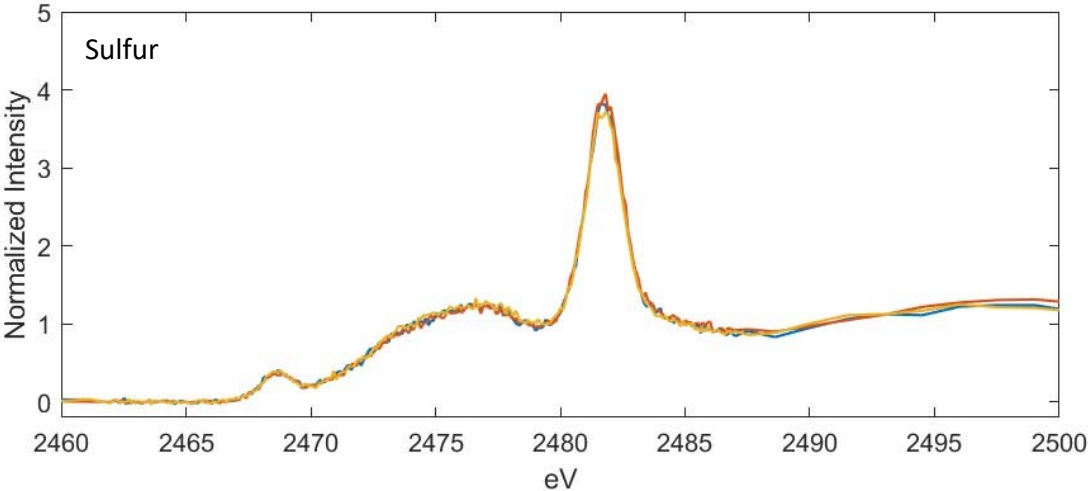
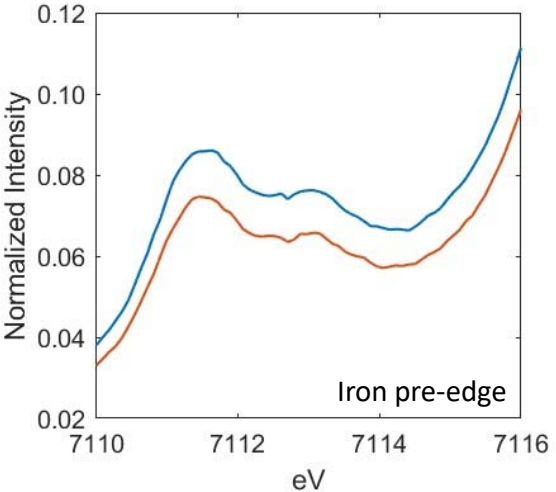
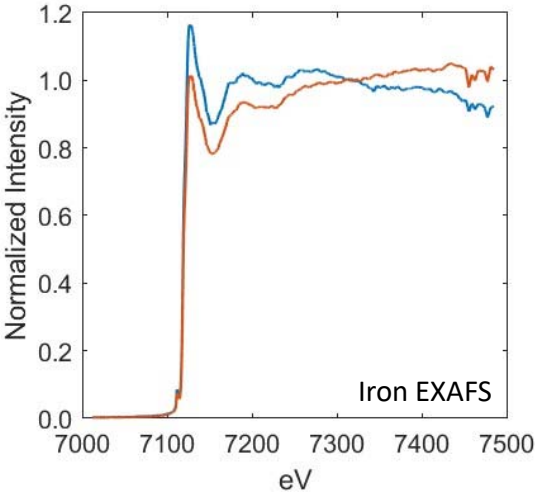
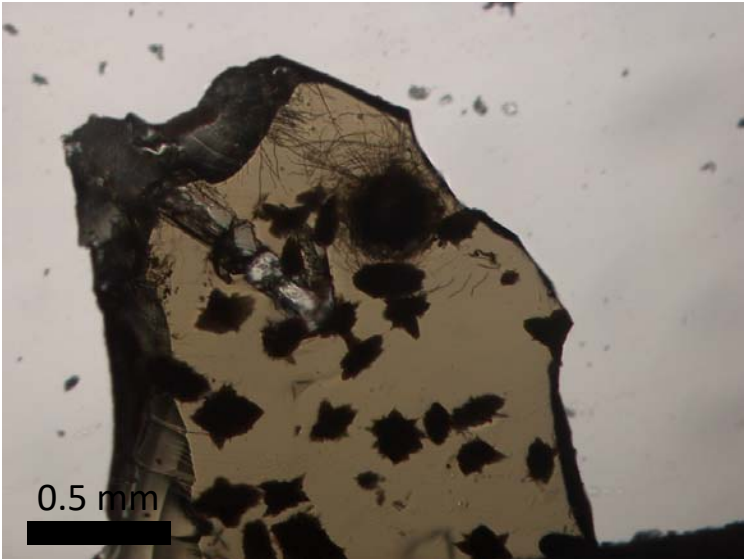




CY16-60

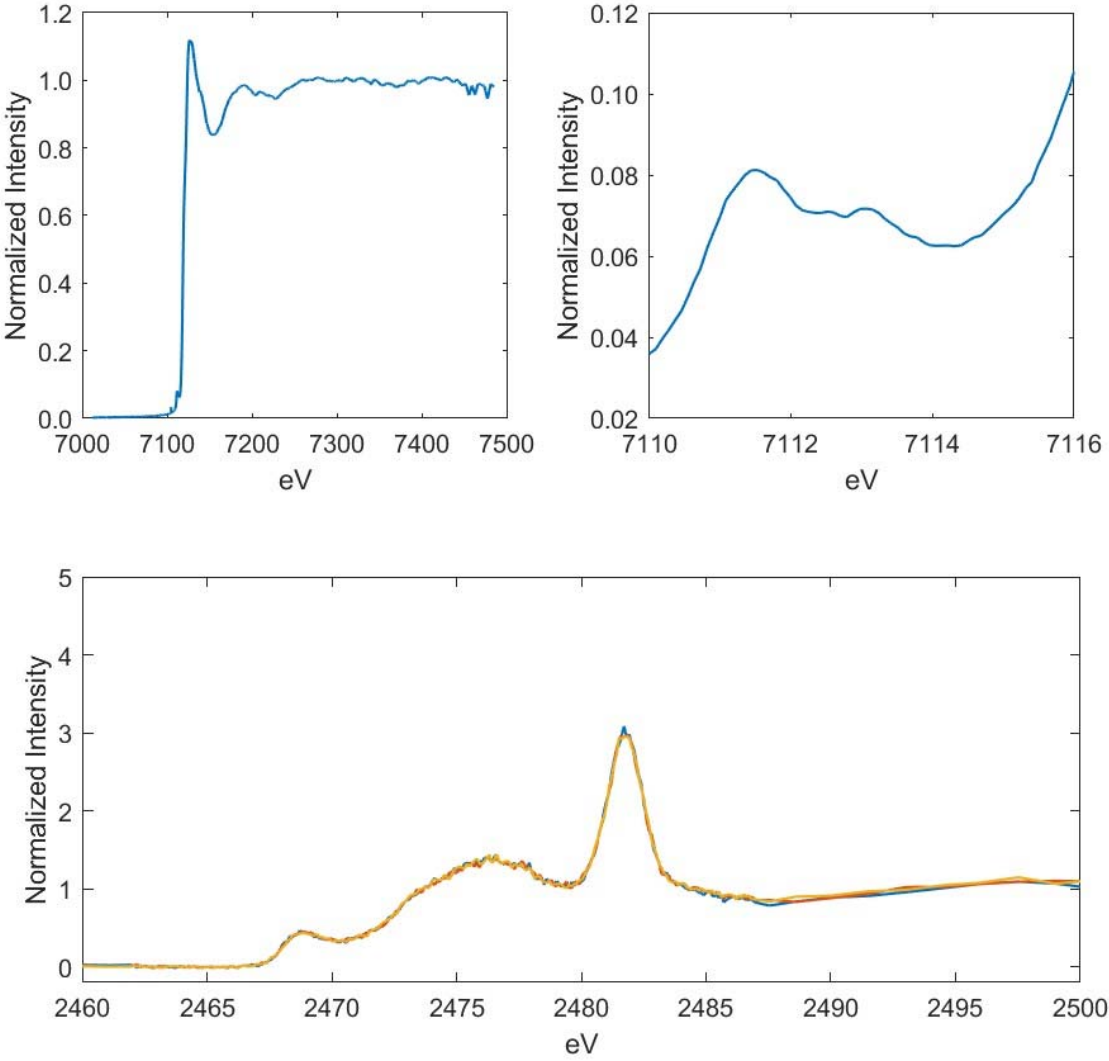
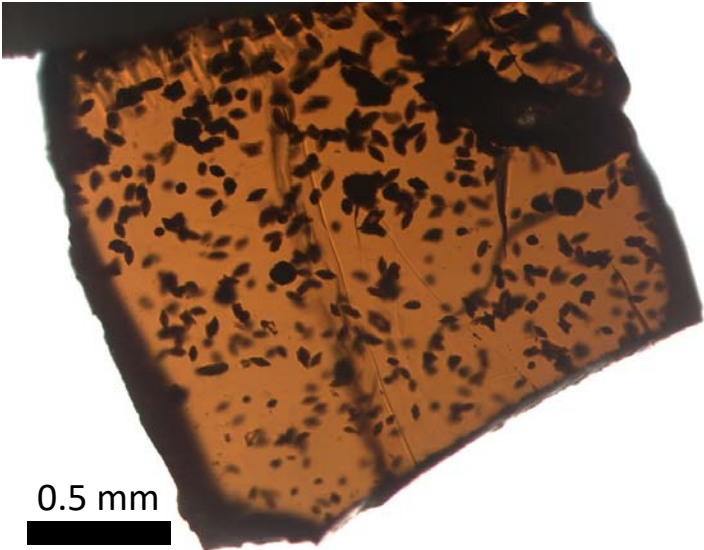


CY16-64



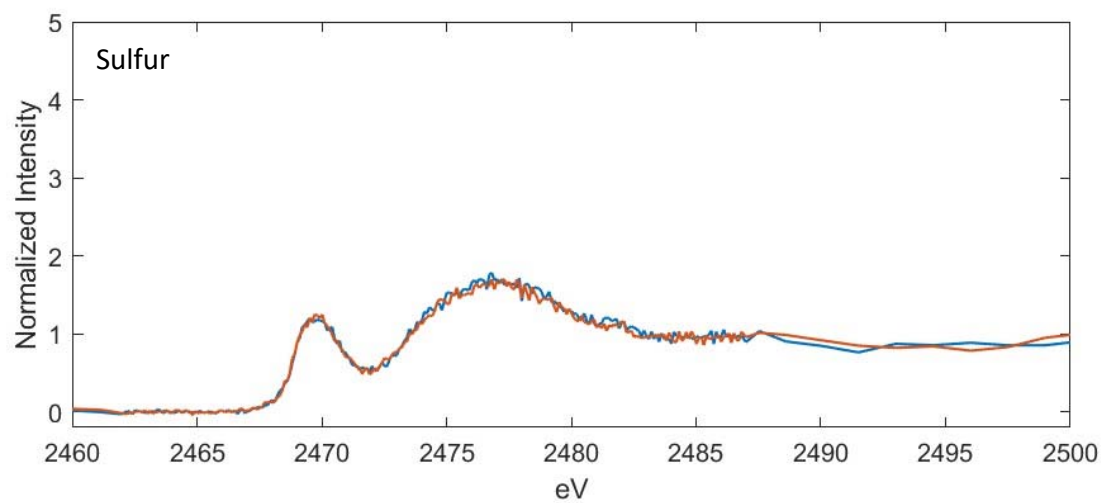
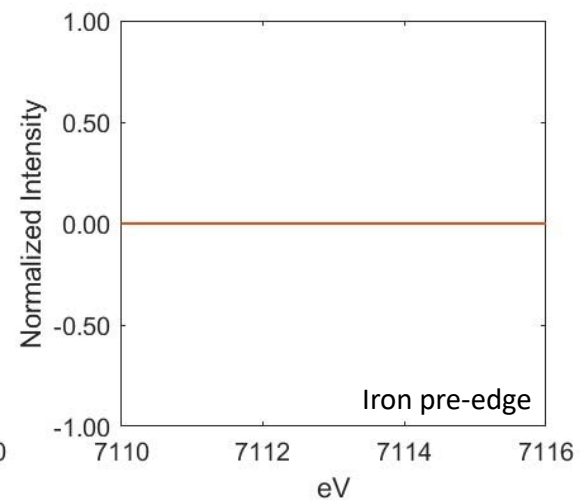
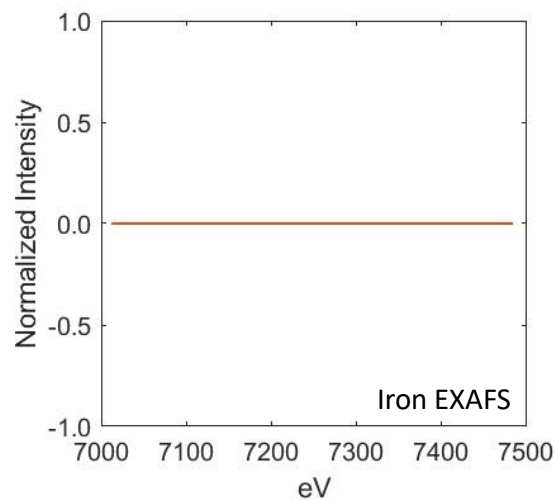
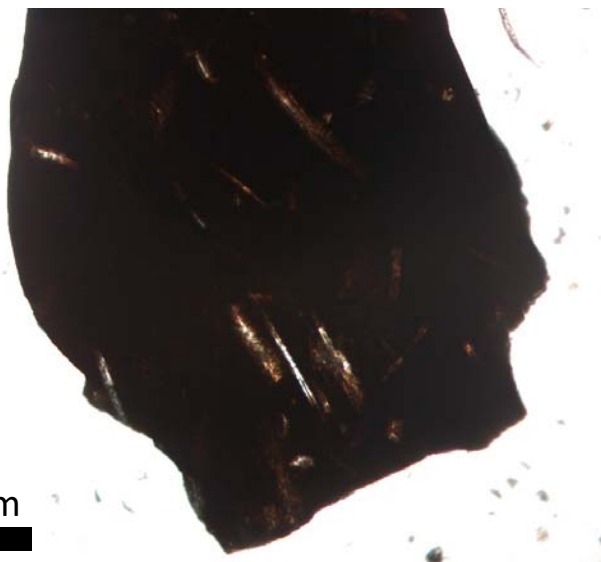


ET-06-02

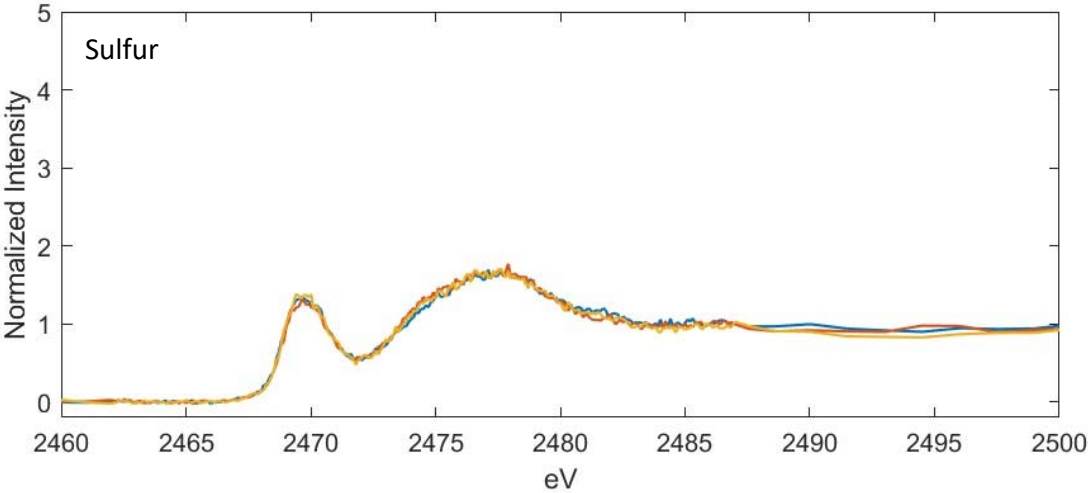
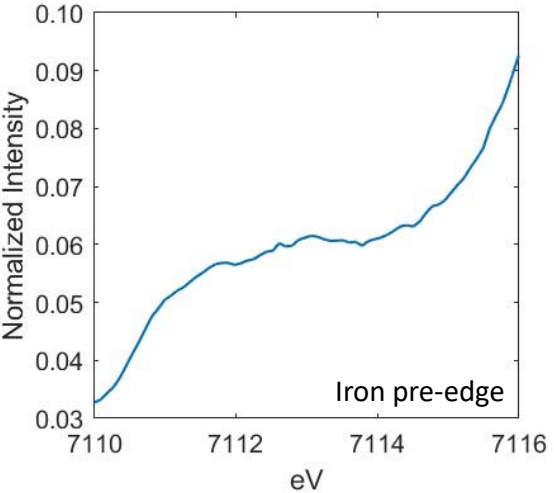
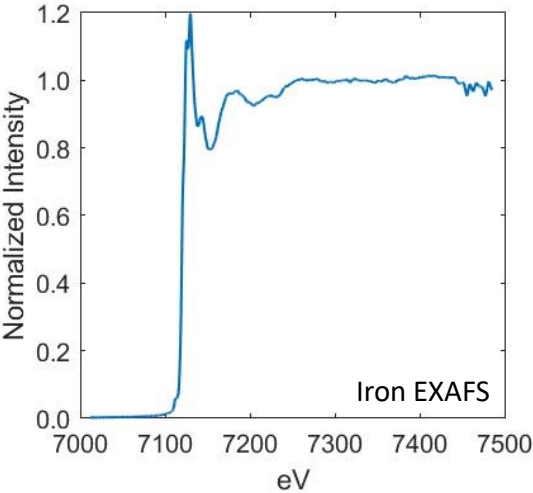
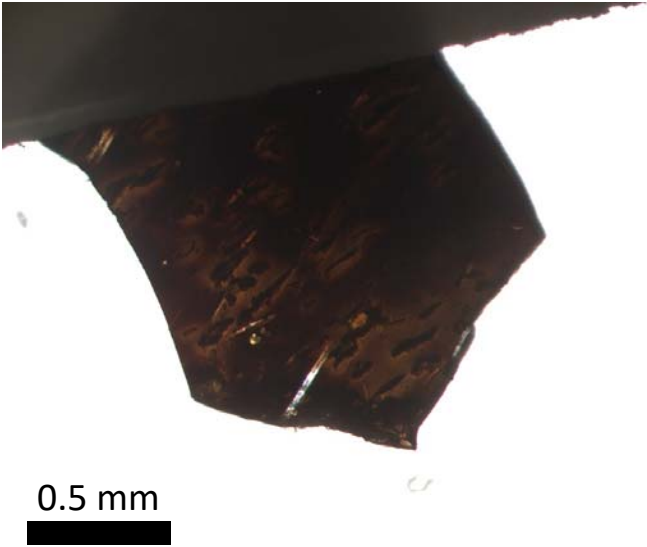


HS-12-12  
(altered)

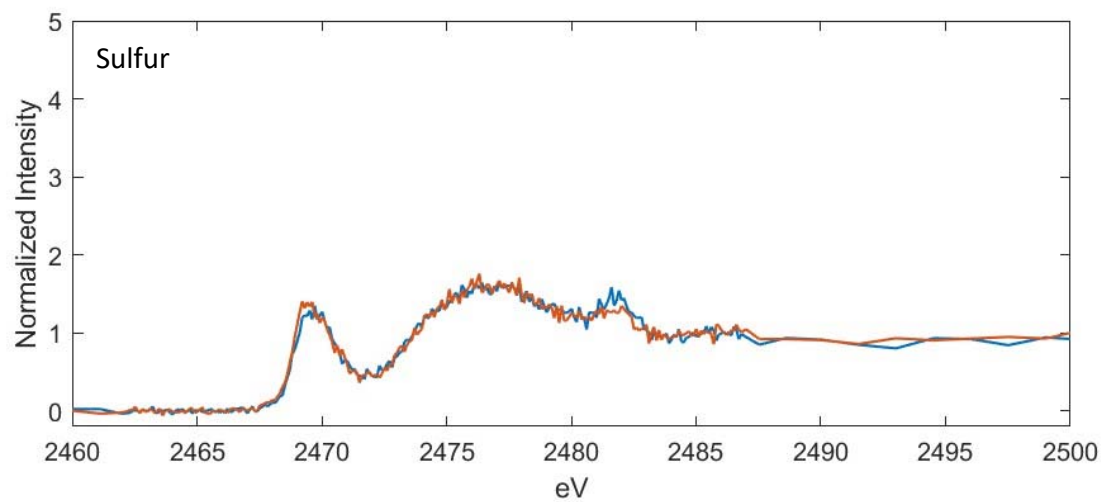
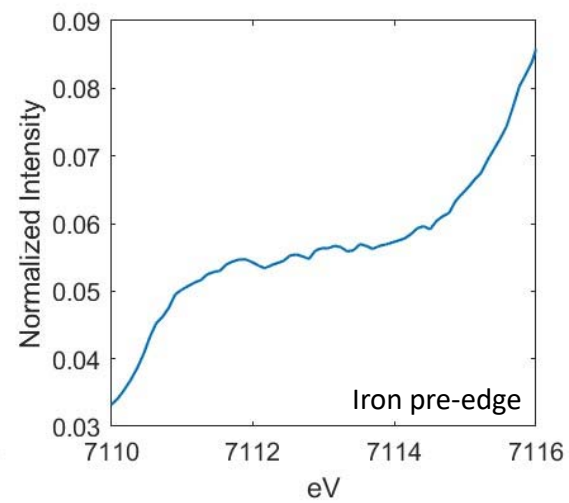
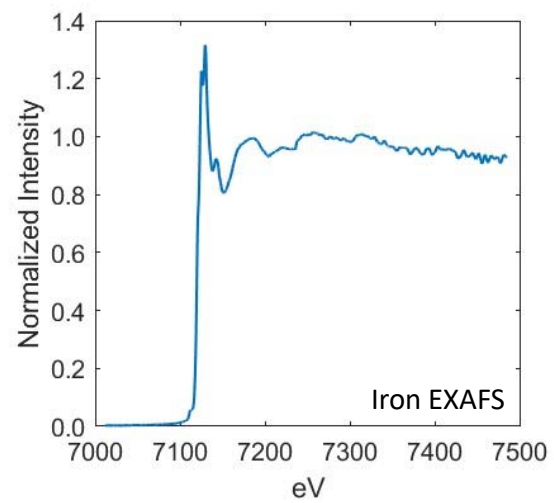
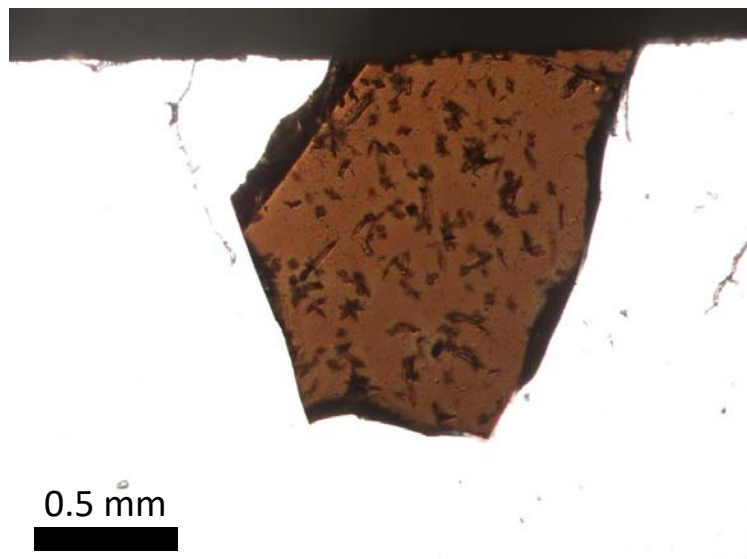
0.5 mm



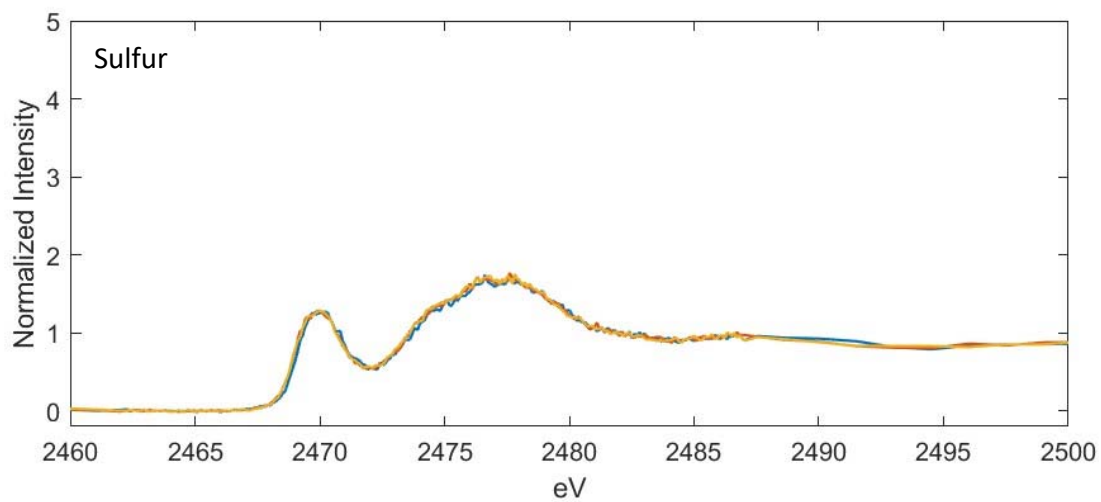
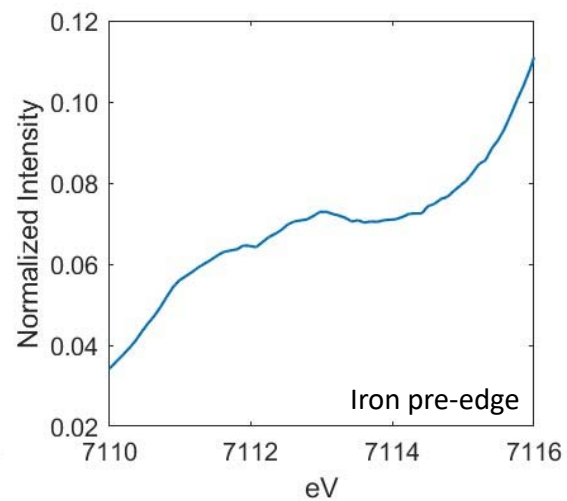
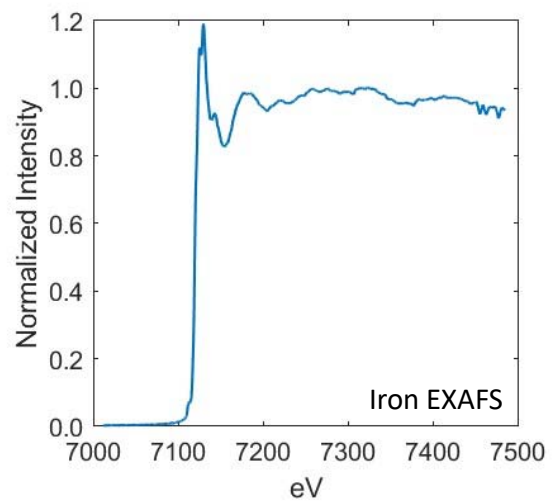
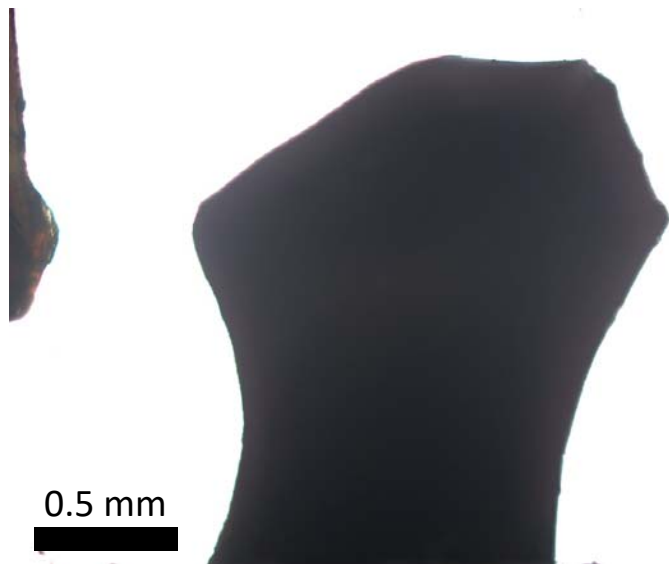
CY17-AR-4  
(altered)



CY18-PR-13  
(altered)



CY17-PR-24  
(altered)



CY17-PR-35  
(altered)

